Degree Project in Technology

Second cycle, 30 credits

Catenary geometry optimization for curved track

Lateral alignment patterns improving contact distribution

WILLE VIMAN VESTBERG

Catenary geometry optimization for curved track

Lateral alignment patterns improving contact distribution

WILLE VIMAN VESTBERG

Master’s Programme, Applied and Computational Mathematics, 120 credits
Date: February 15, 2025

Supervisors: Bastian Schick, Mattias Sandberg, Peter Larsson
Examiner: Mattias Sandberg
School of Engineering Sciences
Host company: Trafikverket
Swedish title: Optimering av hängverksgeometri för kurvor
Swedish subtitle: Trådföringsmönster för förbättrad kontaktfördelning

Abstract

This project's birth is a FEM based model for studying the contact forces between pantograph and contact wire on an electric rail vehicle. The real contact wire is made of copper and is usually placed directly above the railway. Studying the pantographs' interaction with the contact wire is vital in order to be able to e.g. ensure a reliable contact between pantograph and contact wire or to predict wear of the contact strip, which is usually made of carbon. Before building such a model the geometry of the bearing structure needs to be defined, this is given by tables and formulas defined by Trafikverket. The guidelines include distance between bearing posts, maximum dropper distance, maximum stagger, etc.

My task was to investigate and build an explicit model for the distribution of the frequency of contact points from the contact wire onto the pantograph in curved segments. When this distribution was all set a study was performed with the aim of finding an optimal lateral wire alignment (stagger) to enable a smooth distribution of contact frequency. This was solved using both Gradient Descent and gradient-free optimization techniques.

Finally a model that furthermore took into account the span lengths and the wind's effect on the positioning of the contact wire was made with the aim of finding a distribution of staggers and span lengths that resulted in a smooth distribution while still electing solutions with longer span lengths and making sure the wind criteria was fulfilled.

Keywords

Gradient Decent, Gradient-free optimization, Overhead Catenary Line, Railway Electrification, Pantograph, Carbon-strip, MATLAB.

Commonly used acronyms and abbreviations

- **TRV** - Trafikverket

- **CW** - Contact wire

- **SE** - Superelevation, the inclination angle used in curved segments.

- **GA** - Genetic algorithm, gradient-free stochastic optimization algorithm that mimics the process of natural selection.

Sammanfattning

Bakgrunden till detta projekt är en FEM-baserad modell för att studera kontaktkrafterna mellan strömavtagaren och kontakttråden hos elektriska spårfordon. Kontakttråden är tillverkad av koppar och är vanligtvis placerad direkt ovanför spåret. Att studera strömavtagarens interaktion med kontaktledningen är avgörande för att till exempel kunna säkerställa tillförlitlig kontakt mellan strömavtagare och kontakttråd eller att förutsäga slitaget på strömavtagarens slitskena, som vanligtvis är tillverkad av kol. Innan en sådan modell kan byggas behöver bärstrukturens geometri definieras, vilket anges av tabeller och formler som tas fram av Trafikverket. Riktlinjerna inkluderar avståndet mellan bärstolpar, maximalt avstånd mellan bärtrådar, maximal sidoförskjutning (stagger) med mera.

Min uppgift var att undersöka och bygga en explicit modell för fördelningen av frekvensen av kontaktpunkter från kontakttråden på strömavtagaren i svängda sektioner. När denna fördelning var fastställd genomfördes en studie med syftet att hitta en optimal sidoförskjutning (stagger) av kontaktledningen för att möjliggöra en jämn fördelning av kontaktfrekvensen. Detta löstes med hjälp av både gradientbaserade och gradientfria optimeringstekniker.

Slutligen skapades en modell som även tog hänsyn till spannlängder och vindens påverkan på kontaktledningens läge, med målet att hitta en fördelning av sidoförskjutningar och spannlängder som resulterade i en jämn fördelning. Samtidigt prioriterades lösningar med längre spannlängder, och man säkerställde att vindkriterierna uppfylldes.

Acknowledgments

I would like to express sincere gratitude to my supervisors, Bastian Schick and Mattias Sandberg, at KTH, for their invaluable guidance and support throughout this master thesis. I am also grateful to Peter Larsson, my supervisor from Trafikverket, for his insightful comments and expertise. Their encouragement and expertise have been instrumental in the successful completion of this thesis.

Contents

List of Figures

List of Tables

Chapter 1

Introduction

1.1 The catenary-pantograph system for electrified railways

The catenary-pantograph system is a critical component for powering electric trains. It consists of an overhead wire system (catenary) and a pantograph mounted on top of the train. The catenary wire is suspended with precision to maintain a consistent height and tension, allowing for smooth energy transfer. The pantograph, equipped with a spring-loaded arm and carbon contact strips, presses gently against the catenary wire to draw electricity, powering the train's motors. This system provides a direct un-interrupted electrical connection between the power source and the train, minimizing energy loss. Unlike diesel-powered trains, which convert fuel into mechanical energy with lower efficiency, electric trains can achieve much higher efficiency in converting electrical energy into motion. Some other advantages of the catenary-pantograph system for powering electric trains are: The reduced cost in the long run, despite the initial build of the system is rather expensive the system requires lower cost of maintenance than diesel engines in the long run making it a more cost-efficient option. The electric engines produce a significantly lower level of noise pollution than the combustion engine do. In low traffic lines, short sections of catenary systems can be used to support battery-electric solutions.

The overhead wire system is a combination of several different elements.

1. **Contact wire (CW)**, this is the wire that will be in contact with the pantograph.
2. **Messenger wire (MW)**, this is the upper wire seen in Figure 1.1. This

wire is the vertical support for the contact wire used in order for an uniform elasticity and height in the contact wire.

3. **Droppers**- The droppers are the vertical wires connecting the CW and MW.
4. **Span** the span is the distance between the posts in the direction of the track.
5. **Stagger (Zig-Zag)** in order to ensure uniform wear and tear of the pantograph the posts in a straight track are placed with an alternating lateral shift, which ensures that the contact wires point of contact on the pantograph is spread uniformly.
6. **Pantograph** - An apparatus mounted on the roof of a rail-vehicle to produce an uplift for the collector strip.
7. **Collector strip**- The carbon strip mounted on the Pantograph that is in direct contact with the contact wire to supply the vehicle with electricity.

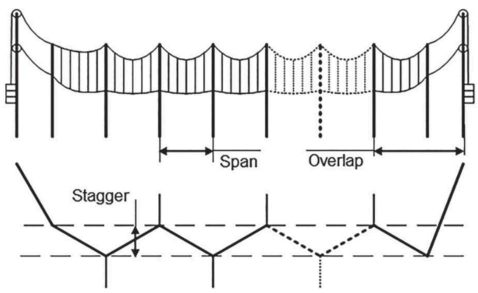

Figure 1.1: Side-view and top-view of a overhead wire system.[1] Straight track.

In curved sections another option for wire alignment than the alternating lateral shift (stagger) is introduced.

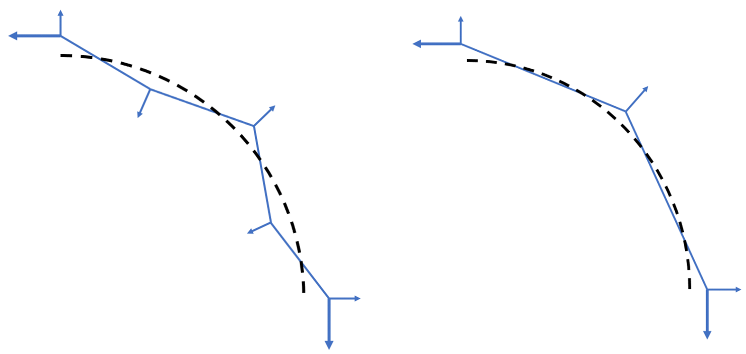

(a) Curve with alternating stagger (b) Curve with unilateral stagger

Figure 1.2: Two different types of **lateral alignment** used in curved sections, corresponding to alternating stagger and unilateral stagger

Unilateral stagger is introduced as a way of enabling the possibility of keeping span lengths longer even in tighter curves while still preserving a good connection between pantograph and contact wire.

1.2 Problem

The main focus in this thesis work will be an in-depth mathematical investigation of the distribution of contact-wear that the contact wire induces on the pantograph in curved sections. In straight track as mentioned in the previous section the point of contact frequency will be uniform, assuming the train is traveling in constant speed, as a direct consequence of the symmetric stagger. In curved sections the geometry is different and as a consequence so will the distribution of the CW contact onto the pantograph be.

The distribution will depend on the value of the stagger, i.e how far normal from the track the wire is suspended, the length of the span, if or if not unilateral stagger is used for specific curve radii etc.

The goal is to produce a distribution showcasing the frequency of contact from CW onto the pantograph for a superposition of different curve radii. This distribution will provide insight and a way for predicting wear of the pantograph in the long run. Studying this distribution will also give the possibility to run optimizations working to smoothening the wear rate by changing parameters such as stagger and span length. This will also be done in this thesis.

A uniform wear distribution implies a decreased need for pantograph replacement in the long run. But there is also an important trade-off with span lengths to mention. Building the bearing posts is the most expensive part of catenary system construction, and longer span lengths means fewer posts. So, the goal is to find a configuration of staggers that produce a smooth distribution of contact points while still making sure span lengths can be kept longer. It is also important to make sure that two structural limitations are fulfilled. These limitations are wind displacement and lateral tensile force. According to TSI energy document [2] the deviation from the center of the track shall not exceed 0.4 m to avoid so-called dewirement, where the CW slides of the side of the pantograph. And according to TRV [3] the Lateral force should be within [70, 900 N].

Chapter 2

Mathematical theory

Firstly gradient descent was used in order to find the optimal stagger values while keeping span lengths constant.

Later the model also accounts for the scenario with hard wind affecting the position of the CW while wanting to make the span lengths as long as possible. The function to minimize becomes more complex and Black-Box optimizers such as Genetic algorithm and Pattern search are used.

Gradient descent is an iterative optimization algorithm used to minimize a function. The core idea of gradient descent is to adjust model parameters iteratively in the direction of the negative gradient of the loss function with respect to the parameters. This adjustment reduces the loss function value, bringing the model closer to an optimal solution.

In order to adequately use the gradient decent method, first the function to be minimized must be defined in a clear way.

Since TRV. currently define their stagger tables using 21 different curve radii and each curve radii would correspond to 2 stagger values, the function f to be minimized will be a function mapping

$$f : \mathbb{R}^{42} \to \mathbb{R}$$

2.1 Geometrical background

For a straight track when we have alternating stagger the wear of the pantograph will be uniform since the frequency of point of contact at each point on the pantograph will be the same within the range of contact, as seen in the bottom of Figure 1.1. In curves this will be different.

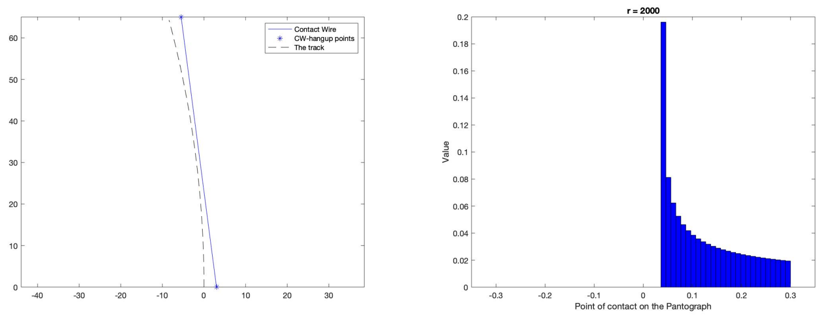

(a) Curve with unilateral stagger. (b) Normalized frequency of contact

Figure 2.1: Top view of curved span and corresponding frequency of contact points on the pantograph

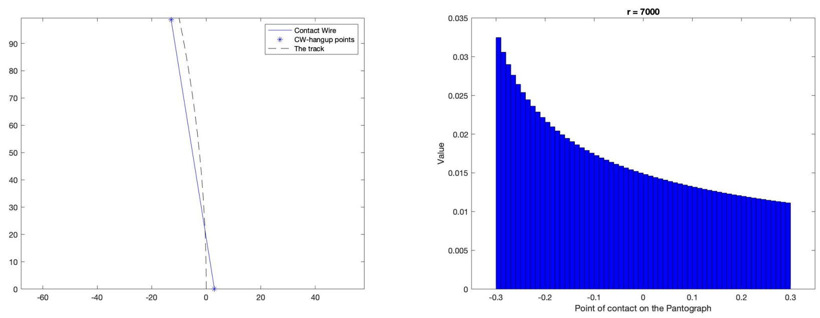

(a) Curve with alternating stagger (b) Normalized frequency of contact

Figure 2.2: Top view of curved track and corresponding frequency of contact points on the pantograph

How the histograms of the distributions are made is explained in more detail in section 3.1. The goal is to create a combined distribution of the points of contact and then finding an optimal configuration of the stagger and Sl values in table 2.1. In Figure 2.3 the distribution of point of contact frequency on the pantograph following the values in Table 2.1 assuming equal length covered for all 21 curve radii is presented.

Radii(m)	s_1 **(m)**	s_2 **(m)**	**Sl**
20000	0.3	-0.3	65
10000	0.3	-0-3	65
9000	0.3	-0.3	65
8000	0.3	-0.3	65
7000	0.3	-0.3	65
6000	0.3	-0.3	65
5000	0.2	0.2	65
4500	0.2	0.2	65
4000	0.2	0.2	65
3500	0.2	0.2	65
3000	0.2	0.2	65
2500	0.2	0.2	65
2000	0.3	0.3	65
1900	0.3	0.3	65
1800	0.3	0.3	65
1700	0.3	0.3	65
1600	0.3	0.3	65
1500	0.3	0.3	65
1400	0.3	0.3	65
1300	0.3	0.3	63
1200	0.3	0.3	62

Table 2.1: Table with stagger and Sl guidelines for the SYT 15/15 system [4]

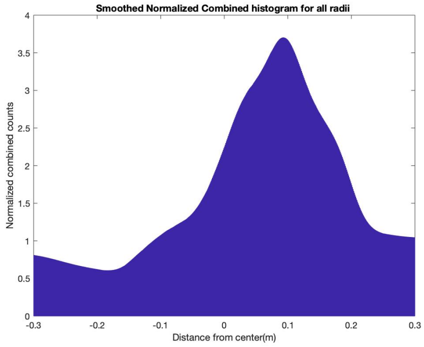

Figure 2.3: Distribution of point of contact frequency on the pantograph

If the distribution in Figure 2.3 is mirrored in x=0 for equal amount of right and left turns the distribution in Figure 2.4

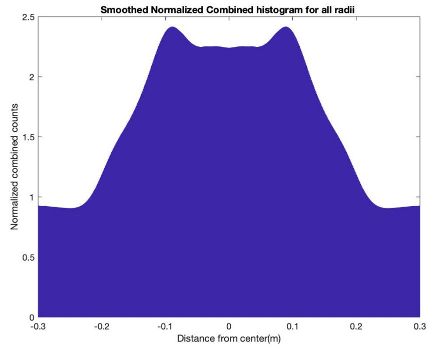

Figure 2.4: Distribution for left and right turns.

These above figures will work as our starting point, showing the distributions that we want to make as uniform as possible. In the following sections I will describe some of the key concepts of the geometrical aspects of building a catenary system for electrical trains.

2.1.1 Stagger

Stagger is the term used for describing the lateral placement of suspension of the contact wire. For straight tracks the suspension is always alternating which ensures a completely uniform wear of the pantograph contact strip. But for curved tracks there is an option to place the CW only on the outside. When the curve radius is very small, alternating stagger is only an option if the span length gets shorter and shorter, but since building the bearing posts is rather expensive, placing all bearing supports on the outside gives constructors the option to keep a longer distances between posts while still ensuring good contact between CW and pantograph. The geometry of alternating stagger and unilateral stagger as well as their corresponding active force diagrams are shown in Figure 2.5.

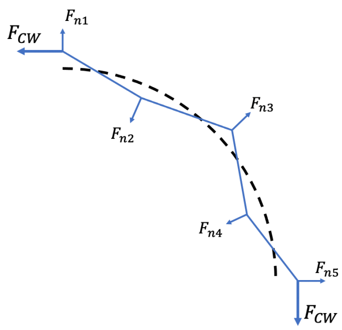

(a) Curve with alternating stagger

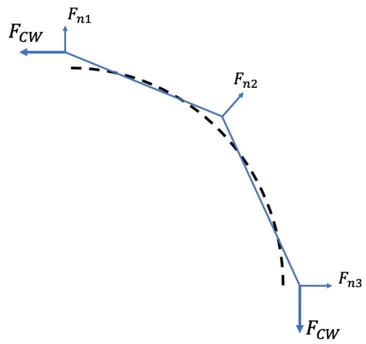

(b) Curve with unilateral stagger

Figure 2.5: Two different types of **lateral alignment** used in curved sections.

2.1.2 Radial component of the tensile force acting on the contact wire (lateral Force, drag)

There are some structural limitations for the normal forces keeping the CW in place, called F_{ni}. These are discussed in [5] [3] and seen in Figure 2.5. The rule of thumb is that the forces should be within the range [70-900 N]. The equations for calculating the forces are presented in the literature and read

$$F_{ni} = F_{tf}^{i} + F_{c}^{i}, \tag{2.1}$$

where the two contributions to the force are due to alternating stagger and the curvature respectively

$$\begin{cases} F_{tf}^{i} = F_{CW}\left(\frac{stag_{i-1}-stag_{i}}{Sl_{i-1}} + \frac{stag_{i+1}-stag_{i}}{Sl_{i}}\right) \\ F_{c}^{i} = F_{CW}\left(\frac{Sl_{i-1}+Sl_{i}}{2R}\right) \end{cases} \tag{2.2}$$

Note that the sign of the first term can alter between negative and positive values, negative values relating to pulling forces in the direction into the curve and vice versa, this is illustrated in Figure 2.5a.

2.1.3 Wind

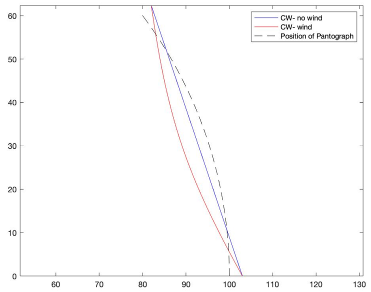

(a) Wind from right

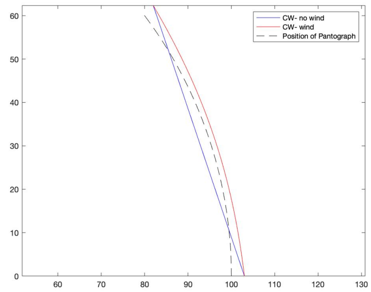

(b) Wind from left

Figure 2.6: Two extreme cases of wind that we need the model to take into account

The equation of the wind is a parabola given by [3]:

$$e(x) = -\frac{1}{2}x(x - Sl) \cdot \frac{p}{F} \tag{2.3}$$

and is the one used by TRV.

1. $p = 6.5$ is the value for p in equation (2.3) provided by TRV. It's the most extreme wind corresponding to a wind speed of approximately 30 m/s. $[p] = \frac{N}{m}$

2. $F = 15000$ N is the tensioning force of the CW

3. Sl is the length of the span

4. x is the distance in line with the track

5. $e(x)$ is the wind caused deviation in the direction normal to the track.

A new stagger configuration that is valid for the most extreme wind will be valid for all winds. The limitation is that the radial distance from the track to the closest point on the contact wire should never exceed 0.4 m.

This is to ensure the compatibilty of the catenary system with standardized European pantograph widths according to the TSI Energy[2]. The reason for the limitation of lateral displacement is to avoid so-called dewirement, where the CW slides off the side of the pantograph. This could lead to catastrophic failures.

The radial distance from the rail to the CW is derived in section 3.1 and is equal to $dist = d(\theta) - r$ hence we have to make sure that

$$|dist \pm e_{max}| < 0.4.$$

2.2 Summary

This section explained the underlying geometrical principles for the CW alignment in catenary systems for curved railway tracks. The next chapter will explain how a model that produces a distribution of frequency of contact from the CW onto the pantograph was made. Optimization techniques will be used to change this distribution into something that is more smooth and resembles an uniform distribution in order to evenly spread the wear of the pantograph contact strip.

Optimization using gradient decent only working on the stagger values will be used and further on using Matlabs powerful Black-Box optimizers when also trying to make the span lengths longer while ensuring the deviations with wind are within the feasible interval.

Chapter 3

Method or Methods

In this chapter it will be explained and motivated how the histogram bin representation of the frequency of contact on the pantograph strip was derived. Also, the mathematical optimization problem of how the overall wear-distribution is made closer to uniform is explained.

3.1 Building the model

To build a model that counts the frequency of point of contact on the pantograph it is vital to first have an explicit model to compute the distance from the origin of the contact strip to the point on the strip with which the CW is in contact with.

The idea is to think of each curve segment as a circle sector with radius R and arc length corresponding to the span length. In curved sections the track will be inclined which is called superelevation. The superelevation angle depends on projected train speed in that section and the curve radius, and there are not any tabulated values for specific superelevation for specific curve radii. Therefore the assumption in this section is that R, the curve radius, will denote the radial distance from the center of the circle segment to the center-point of the contact strip that will coincide with the line normal to the track at the height of the contact strip. See Figure 3.1

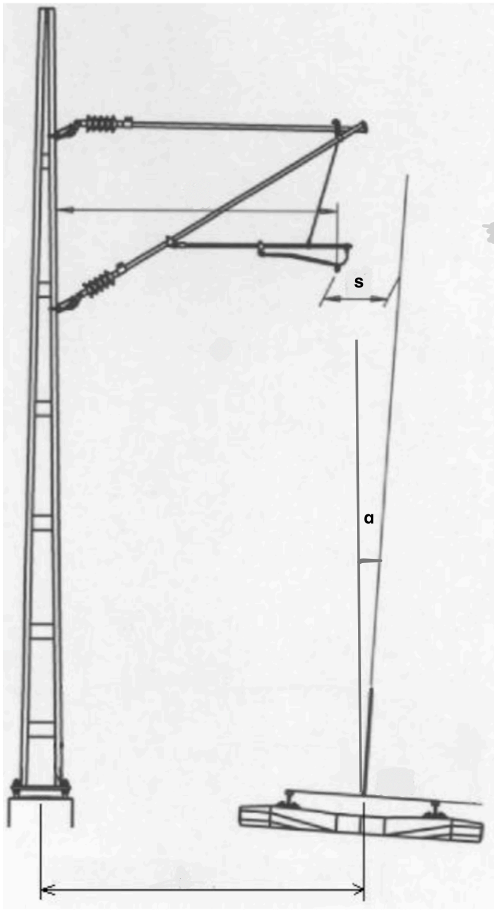

Figure 3.1: Superelevation visualization. [3]

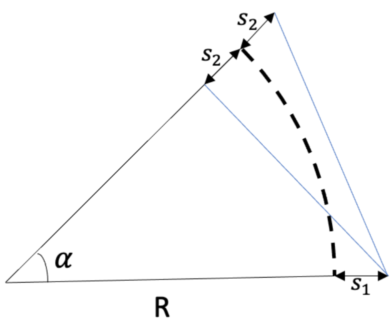

Figure 3.2: Visualization of one Curve Segment, with alternating stagger s_2 is on the inside and with unilateral stagger s_2 is on the outside

The position of the posts in Cartesian coordinates is

$$\begin{bmatrix} x_1 \\ y_1 \end{bmatrix} = \begin{bmatrix} (R + s_1) \\ 0 \end{bmatrix}$$

$$\begin{bmatrix} x_2 \\ y_2 \end{bmatrix} \begin{bmatrix} (R \pm s_2)cos(\alpha) \\ (R \pm s_2)sin(\alpha) \end{bmatrix},$$

depending if the curve has alternating stagger or unilateral stagger and assuming the that the curve starts at $\begin{bmatrix} R \\ 0 \end{bmatrix}$ and $\alpha = \frac{Sl}{R}$.

The line connecting the posts, i.e. the CW, will be a straight line, given by

$$y = kx + m,$$

where k and m are constants.

From now on s_2 is introduced as a variable that takes positive values for unilateral stagger and negative for alternating stagger.

Then the following computations are valid for both cases.

$$\Delta x = (R + s_1)cos(0) - (R + s_2)cos(\alpha),$$

$$\Delta y = (R + s_2)sin(\alpha) - (R + s_1)sin(0),$$

The value of k is given by the slope

$$k = \frac{\Delta y}{\Delta x}$$

and m is the intersection point with the y axis, given by

$$m = -\frac{\Delta y}{\Delta x} \cdot (R + s_1),$$

since y is 0 when $x = (R + s)$.

Hence

$$y = kx - k(R + s_1)$$

in polar coordinates this translates to:

$$d(\theta)sin(\theta) = k \cdot d(\theta)cos(\theta) - C$$

where

$$\begin{cases} C = k(R + s_1), \\ \theta \in [0, \alpha], \end{cases}$$

hence the distance from the origin to a point on the chord connecting the two posts is given by

$$d(\theta) = \frac{-C}{sin(\theta) - kcos(\theta)}, \theta = [0, \alpha].$$

And the distance from the origin to the arc is simply R.

hence the contact strips' point of contact with the CW as a function of the angle will be the distance between the circle arc and the straight line connecting the posts

$$d(\theta) - R.$$

Since we are interested in how the span length Sl, stagger (s_1, s_2) and the Radius R affects this distance we call this

$$dist(Sl, stag, R) = d(\theta) - R.$$

3.2 Histogram representation

θ is divided into a fixed amount of steps and then the dist-data is represented as a histogram where each point on the x-axis corresponds on a point on the contact strip and and the normalized counts in each bin represent how big portion of the time the CW is in contact with that exact position on the pantograph.

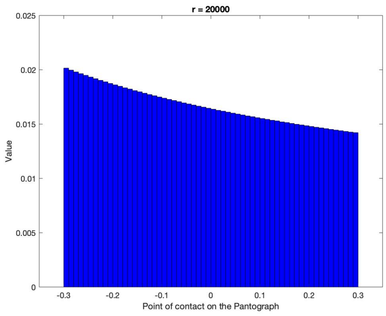

(a) R = 20000

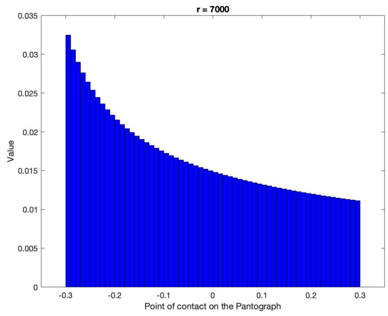

(b) R = 7000

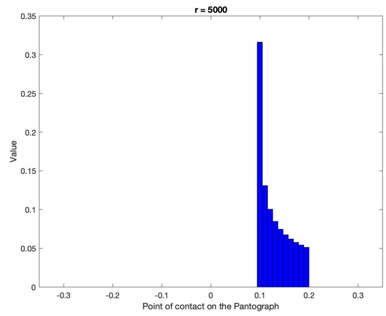

(c) R = 5000

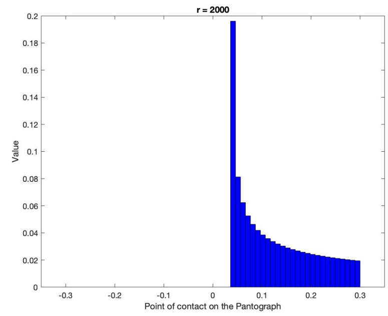

(d) R = 2000

Figure 3.3: A selection of histograms of point of contact frequency for different curve radii.

Note that I use the same fixed bin width of 0.01 m for all histograms since this in a good order relates to the width of the actual contact wire that is 0.0125m for the SYT 15/15 system. This can of course be changed, but the impact is negligible.

3.3 Combining the Histograms

To compute a combined distribution of all 21 curve radii a discretization of the x-axis is made from the minimum dist-value for all 21 curve radii to the maximum. All bins from the 21 different curve radii will fall in one of these bins since those individual bins are calculated with the same discretization of the x-axis. The fixed discretization I use in this report is with a fixed bin width of 0.001 m for distribution presentation, and 0.01 m in the optimizations for computational speed reasons, since this decreases the number of data points needed to create a representative distribution.

Since the same number of data points are used to create each histogram distribution for all separate curve radii and the bin width is constant for all, the weight from each separate histogram is equal. This can later be modified in case we know the portion of the length of total train network for specific curve radii.

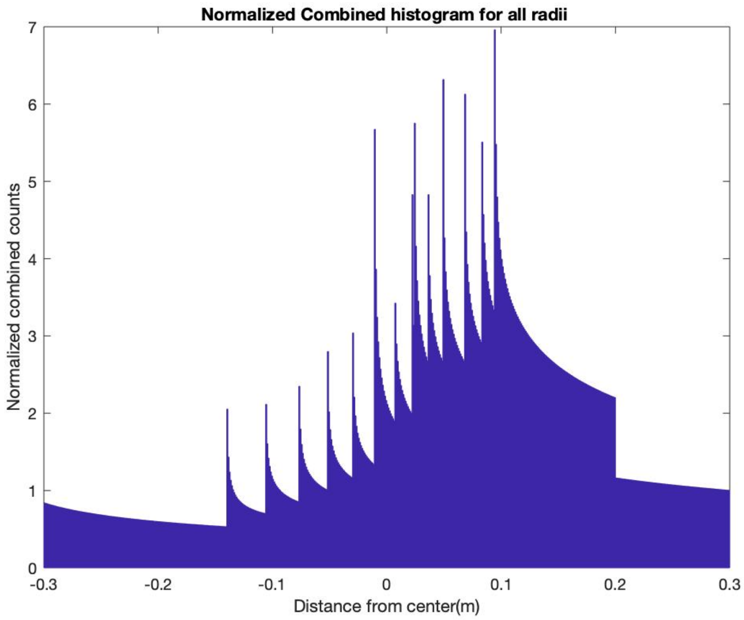

Figure 3.4: Combined distribution without smoothing for all 21 curve radii, bin width 0.001 m

The distribution for the first 6 curve radii in Table 2.1 will cover the entire domain [-0.3, 0.3] since they use alternating stagger. For the remaining 15, the peak of the histogram will lie at the innermost point on the pantograph as explained in previous section. Looking at Figure 3.4, the 13 peaks are clearly visible and the remaining 2 lie in adjacent bins, these peaks will inevitably contribute to the overall wear of the pantograph. Those individual peaks cover approximately 0.3 % of the total Pantograph width and a more interesting and extensive studies can be made with a smoother representation of the distribution that still preserves the overall trends. Therefore a smoothening is performed on this distribution.

The combined histogram distribution is smoothed using Gaussian smoothing. Gaussian smoothing is a technique used to reduce noise and create a smoother representation of a histogram distribution. It involves applying a Gaussian filter, which uses a bell-shaped curve, to weight the values of the histogram. Each bin's value is replaced with a weighted average of itself and its neighboring bins, with closer neighbors contributing more to the average. This process preserves the overall shape and trends of the histogram while eliminating sharp fluctuations, making it particularly useful for visual clarity and analysis 3.5. This smoothening can also be assumed to represent the effect of small variations that are constantly present in the real system. From here on distributions will always be smoothened, both when presented and in the optimizations further on.

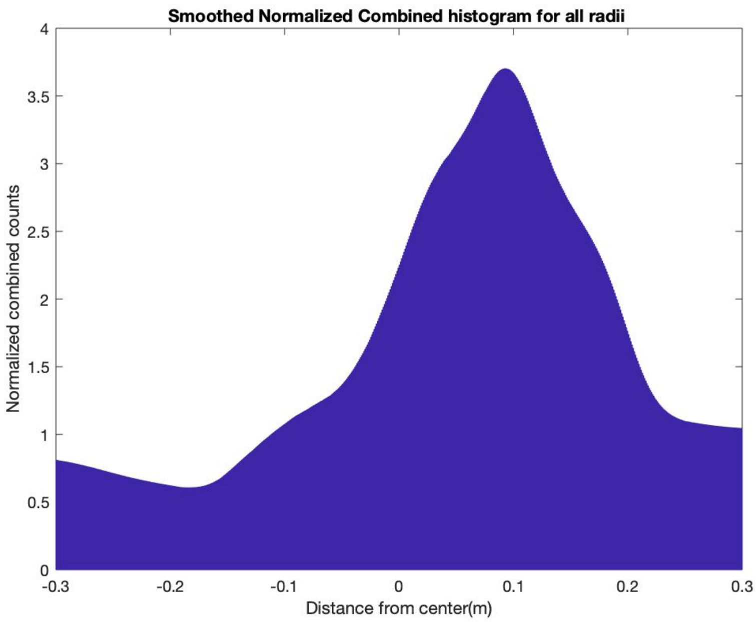

Figure 3.5: Distribution in Figure 3.4 after Gaussian smoothing, called P(x)

If we further more assume the train will turn the same amount to the left and to the right we can obtain an adequate distribution for this case by realizing that right and left turns are symmetrical. Hence

$$P_{right}(x) = P(-x) \tag{3.1}$$

and Figure 3.6

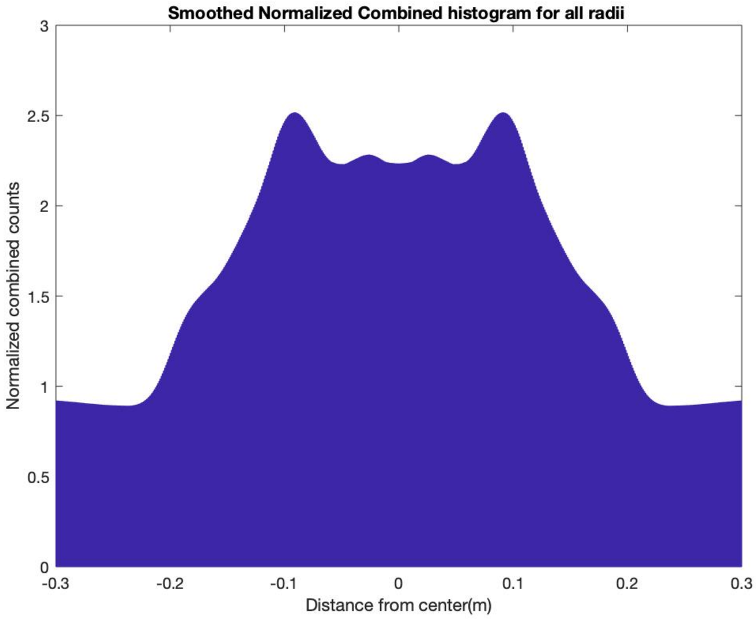

Figure 3.6: Distribution P(x) + P(-x)

3.4 Using data of real world railway network from TRV

TRV provided me with data containing the proportion of the total length for each curve in the Swedish railway network. These are presented Table in 3.1. The combined distribution of point of contact frequency for this case will look something like Figure 3.7 and Figure 3.8.

Radii	Proportion of total length in railway network
∞	0.7985
20000	0.0057
10000	0.0025
9000	0.0008
8000	0.0023
7000	0.0021
6000	0.0038
5000	0.0063
4500	0.0036
4000	0.0083
3500	0.0216
3000	0.0262
2500	0.0261
2000	0.0131
1900	0.0043
1800	0.0080
1700	0.0040
1600	0.0078
1500	0.0143
1400	0.0043
1300	0.0082
1200	0.0282

Table 3.1: Table with radii och rounded proportions.

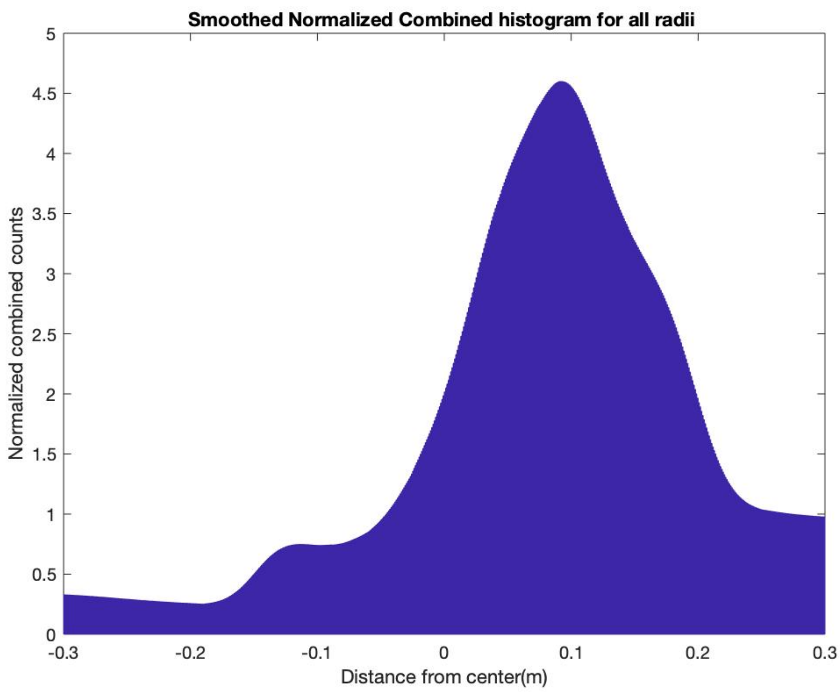

Figure 3.7: Combined distribution using TRV network data.

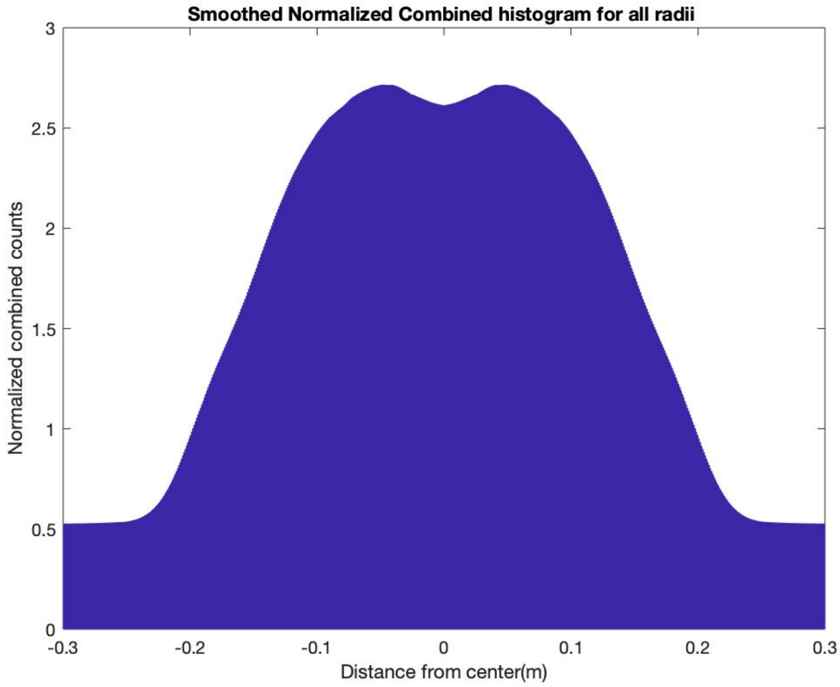

Figure 3.8: Distribution P(x) + P(-x) using TRV network data.

In reality,, electrical vehicles will not only travel in curved sections but on straight track as well. The distribution for straight track is uniform over the range [-0.3 0.3], which is the alternating stagger used for straight track. Adding this contribution of straight track to the distribution gives a distribution that looks like Figure 3.9.

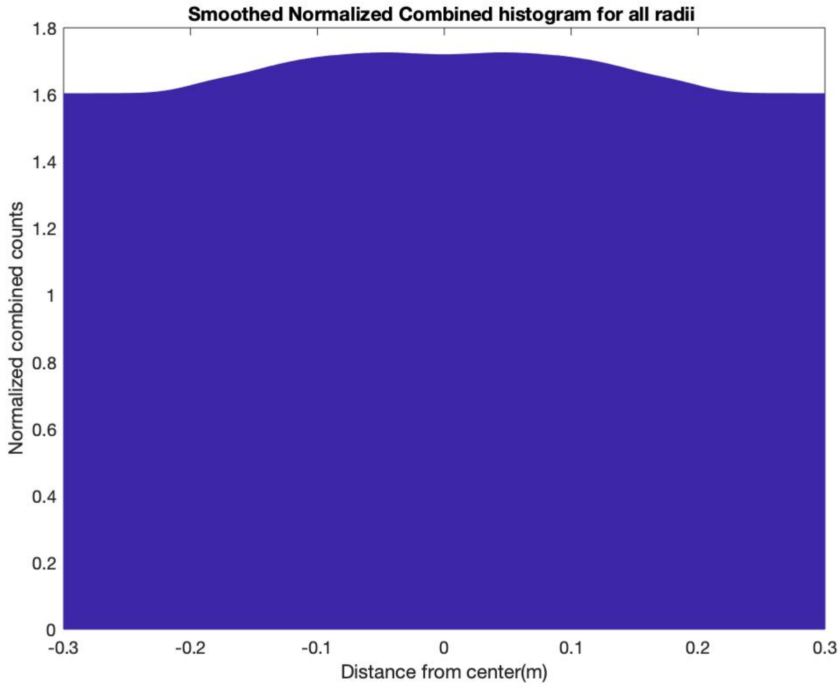

Figure 3.9: Combined distribution using TRV. data adding straight track.

The wear pattern in Figure 3.9 can be compared to fully worn collector strips seen in Figures 3.10 and 3.11. The wear is most prominent in the region $\pm 0.08m$ away from the center and is least prominent further out.

Figure 3.10: Picture of an old Pantograph

Figure 3.11: Picture of an old contact strip (bottom) and a new one (top) where the wear pattern is apparent.

3.5 Optimizing the wear

Figures 3.5 and 3.6 show two distributions telling us the concentration of points of contact on the contact strips. The patterns of these distributions are strongly dependent on the stagger configuration.

The ideal distribution is the uniform distribution, as in Figure 3.12, since this would mean that each part of the contact strip is worn out the same amount, limiting the need for contact strip replacement. Hence, one function to minimize would be

$$f(\vec{S}) = \int_{-\infty}^{\infty} \Big(P(\vec{S}, x) - U(x)\Big)^2 dx = ||P - U||_2^2 \tag{3.2}$$

where

$$\begin{cases} U(x) = \frac{1}{|X|}, x \in X \\ U(x) = 0, \textit{else}, \end{cases}$$

$$\begin{cases} \int_x P(x)dx = \int_X U(x)dx = 1 \\ \vec{S} = [s_1^1, s_2^1, ..., s_1^{21}, s_2^{21}, sl_1, ..., sl_{21}] \end{cases}$$

and X is the ideal nominal width of the working zone on the contact strip which is set to [-0.3, 0.3] for the work in this thesis. Since a value $f = 0$ would correspond to $P = U$, and that is our goal.

Since an analytical representation for the distribution $P(x)$ does not exist in practice the distributions are represented in Bin-representation where we are computing the L2-norm in equation (3.2) as the approximated sum

$$\sum_i \left(P(\vec{S}, x_i) - U(x_i)\right)^2 \cdot \Delta x.$$

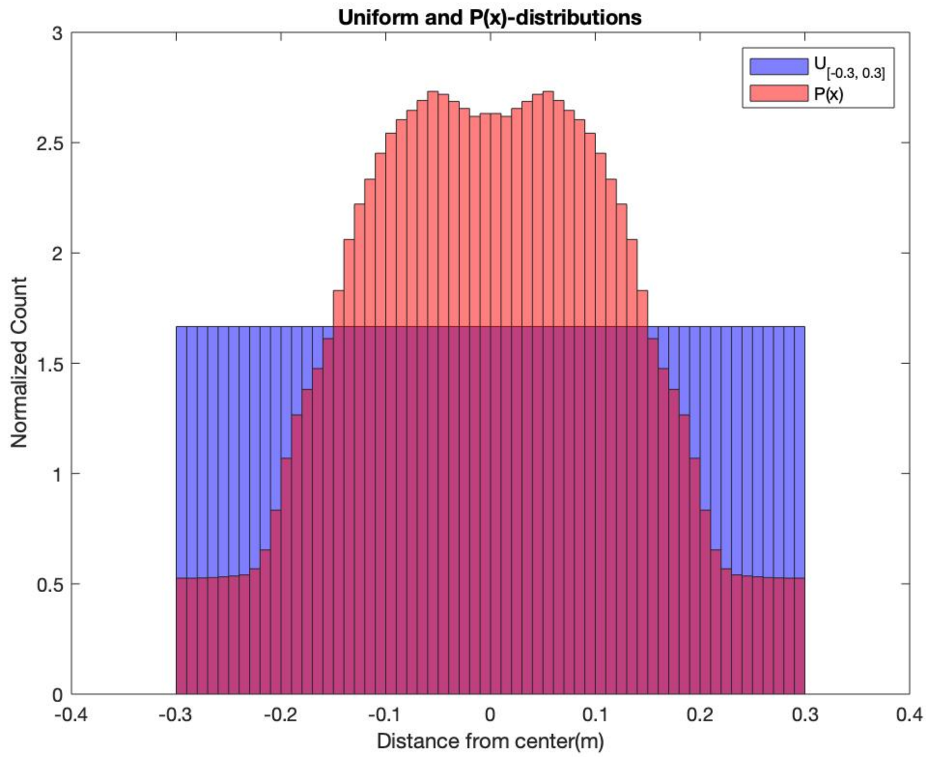

Figure 3.12: Visualization of the Bin-representation of the functions U(x) and P(x)

3.6 Building the Gradient optimizer for the stagger

Let us write the function to minimize

$$f(\vec{s1}, \vec{s2}) = L2^2, \tag{3.3}$$

where L2 is the L2-norm:

$$||P - U||_2,$$

and U(x) = $\begin{cases} \frac{1}{B-A} & \text{for } A \leq x \leq B, \\ 0 & \text{else .} \end{cases}$

$(\vec{s1}, \vec{s2})$ are vectors containing the stagger information relating to columns 2 and 3 in Table 2.1.

The objective is to minimize f in Equation (3.3). In the table from TRV we have 21 different curve radii. Hence, the function f will be a function

$$f : \mathbb{R}^{42} \rightarrow \mathbb{R}$$

since each curve radius has two relating stagger values s_1 and s_2.

The problem of finding the optimal configuration for the 42 stagger values is solved by using the Gradient Decent Method [6]

$$\vec{S}_{n+1} = \vec{S}_n - \gamma \nabla f(\vec{S}_n),$$

where the gradient is a vector where the ith element is simply

$$\nabla f(\vec{S})_i = \frac{\partial f(\vec{S})}{\partial S_i}.$$

The derivatives are approximated using central difference

$$\nabla f(\vec{S}) = \begin{pmatrix} \frac{f(s_1+\Delta s, s_2, \ldots, s_n) - f(s_1 - \Delta s, s_2, \ldots, s_n)}{2\Delta s} \\ \frac{f(s_1, s_2+\Delta s, \ldots, s_n) - f(s_1, s_2 - \Delta s, \ldots, s_n)}{2\Delta s} \\ \ldots \\ \ldots \\ \frac{f(s_1, s_2, \ldots, s_n+\Delta s) - f(s_1, s_2, \ldots, s_n - \Delta s)}{2\Delta s}. \end{pmatrix}$$

Convergence to local optima is always guaranteed with gradient descent as long as the function f is smooth, ∇f is Lipchitz-continuous and the tuning parameter γ is small enough. Since little is known about our function f, for now the assumption that ∇f is Lipchitz-continuous is made, meaning the difference in gradient values is bounded.

3.7 Modified Gradient Decent

To solve the issue where the points of contact on the pantograph may fall outside the feasible range with strong wind present, the GD algorithm can be slightly modified if necessary to evaluate the maximum distance from the center of the pantograph at each iteration and look for solutions not as extreme in case the wind and lateral force criteria are not fulfilled for that radius. The variable wind assigned in the function WIND(**S**) in the pseudo-code below simply gives the index for the staggers in the vector **S** that violate the wind criteria. Those specific elements of the vector **S** are recalculated with one Gradient decent-step with a decreasingly smaller and smaller search parameter γ until the criteria are met. This way we get an algorithm that still looks for solutions in the direction of the steepest descent but ensure the wind criteria are fulfilled. The reasoning for the lateral drag force is analog so its algorithm is not shown separately.

Algorithm 1 Iterative Update Algorithm that ensures wind criteria is not violated

Input: $\mathbf{S}_{\mathrm{i}}, \gamma$
Output: $\mathbf{S}_{\mathrm{i+1}}$
while $\mathtt{wind} \neq \emptyset$ **do** $-$ _
$\mathbf{S}_{upd}^{\mathtt{wind}} \leftarrow \mathbf{S}_{i}^{\mathtt{wind}} - \gamma \cdot \nabla f(\mathbf{S}_{i}^{\mathtt{wind}})$
$\mathtt{wind} \leftarrow \mathit{WIND}(\mathbf{S}_{upd})$
$\gamma \leftarrow \gamma/2$
end
$\mathbf{S}_{i+1} = \mathbf{S}_{upd}$

3.8 Black-Box optimization

In order for our optimized stagger and span length configurations to be feasible for practial applications, we need to make sure that no point of contact exceeds 0.4 m even when we assume we have worst case scenario wind acting on the CW. Furthermore, longer span lengths are always preferable since it means fewer posts need to be built and they are the most expensive part of the catenary system to build. And finally, the lateral forces pulling the CW in place needs to be within the acceptable range [70, 900 N]. All of these parameters can be realized mathematically as penalty-terms.

Let us write a function f to minimize which includes all of these parameters while still making the point of contact distribution as uniform as possible.

$$\begin{aligned}
&f(\vec{S}) = \int_{-\infty}^{\infty} \Big((P(\vec{S};x) - U(x))\Big)^2 dx + \\
&K_{wind} \cdot \int_{-\infty}^{-0.4} \Big((P_{maxwindleft}(\vec{S};x) - 0)\Big)^2 dx + \\
&K_{wind} \cdot \int_{0.4}^{\infty} \Big((P_{maxwindrigth}(\vec{S};x) - 0)\Big)^2 dx + \\
&K_{sl} \cdot \sum_{l} \frac{1}{Sl_l} + K_p \cdot \sum_{i} \mathbb{I}(F_{ni})
\end{aligned} \tag{3.4}$$

where $\mathbb{I}(F_{ni})$ is the indicator function

$$\mathbb{I}(F_{ni}) = \begin{cases} 1, if, F_{ni} \notin [70, 900] \\ 0, else \end{cases}$$

and

$$F_{ni}$$

is the calculated lateral force according to Equation (2.1), and we can call the four last terms penalty terms. Choosing a large enough value for the constant K_{wind} will ensure that those integrals become zero meaning that the distribution of contact will never fall outside of the feasible domain even when strong wind is occurring. $P_{maxwindleft}$ and $P_{maxwindrigth}$ are the distributions of point of contact with maximum wind added to the position of the CW as presented in Figure 2.6. Furthermore, choosing a large enough value of the constant K_{Sl} will make the optimization favor solutions with larger span lengths, and choosing a large enough value of K_p will cancel solutions that violate the criteria for the lateral force.

Since there still isn't any explicit function for the distribution P, the function f will be treated as the sum

$$
\begin{aligned}
&f(\vec{S}) = \sum_i \Big((P(\vec{S};x_i) - U(x_i))\Big)^2 \Delta x + \\
&K_{wind} \cdot \sum_j \Big((P_{maxwindleft}(\vec{S};x_j) - 0)\Big)^2 \Delta x + \\
&K_{wind} \cdot \sum_k \Big((P_{maxwindrigth}(\vec{S};x_k) - 0)\Big)^2 \Delta x + \\
&K_{sl} \cdot \sum_l \frac{1}{Sl_l} + K_p \cdot \sum_i \mathbb{I}(F_{ni})
\end{aligned}
\tag{3.5}
$$

where

$$
\begin{cases}
i \in I | x_i < 0.4 \\
k \in I | x_k > 0.4 \\
l = [1, 21]
\end{cases}
$$

The function f in equation (3.5) is calculated using the same Bin-representation as in Figure 3.12. This problem of minimizing f can be treated as a Black-Box problem since the output f, can be monitored for different inputs, $\vec{S}$. Ultimately the values of the parameters in $\vec{S} = [s_1^1, s_2^1, s_1^2, s_2^2, ..., s_1^{42}, s_2^{42}, Sl_1 Sl_2, ..., Sl_{21}]$ determines both the partitioning of x and ultimately the value of f. Hence, $\vec{S}$ is the input and the output is f and thus this problem is well suited for Black-Box optimization. MATLAB offers several different Black-Box optimizers such as Genetic optimizer (GA), Pattern-search and Particle-swarm.

Black-Box algorithms need some constraints of the input and for the sake of this optimization these constraints are set to.

$$
\begin{cases}
S_i \in [-0.4, 0.4] for\ i \in [1, 42] \\
S_i \in [65, \infty) for\ i \in [43, 63]
\end{cases}
\tag{3.6}
$$

3.8.1 Genetic Algorithm

The Genetic algorithm is a stochastic gradient-gree optimizer inspired by the principle of natural selection[7]. How the algorithm works is summarized in the following steps:

1. An initial population is chosen randomly from the set of Boundary conditions (3.6).

2. Fitness scores from the individuals of this population are evaluated in accordance with the objective function.

3. Fitness scores from the individuals of this population are evaluated in accordance with the objective function.

4. Some individuals with the best fitness scores are chosen as parents.

5. The parents pass their information onto the next generation either by mutation, meaning a small random set of changes are performed of the parent, or crossover, meaning two randomly chosen parents mix their vector entries.

The algorithm continues until some stopping criteria are met, e.g. it exceeds the maximum number of iterations or the fitness score gets smaller then some threshold.

The stochastic nature can affect the convergence rate. Some runs may converge quickly to a high-quality solution, while others might take longer because of searching in less promising regions. The stochastic nature of this algorithm also makes reproducing results difficult.

3.8.2 Pattern Search

Pattern search is a gradient-free optimization algorithm provided by MathWorks. Pattern search is a good method since it has some established global convergence theory [8] even though it does not need any gradient information.

An initial guess S_0 is made, this is a manual input and S_0 was chosen as the values from Table 2.1.

At each iteration, i S_i is evaluated in all search directions

$$S_i^j = \begin{cases} S_{i-1} + \omega e_j \\ S_{i-1} - \omega e_j, \end{cases}$$

where e_j is the j^{th} unit vector and ω is called the mesh size, i.e, how far away from the current point is the algorithm looking. If a point where the objective is smaller is found

$$f(S_i) < f(S_{i-1}),$$

then the point is updated and the mesh size is increased by a factor of two (default in Matlab) to cover a broader range of values for the next iteration.

If the poll is unsuccessful, meaning no point where improvement is made is found,

$$S_i = S_{i-1}$$

and the mesh size is decreased by a factor of two two search more locally.

Improvement of the objective function is monitored in Matlab and convergence to stationary point S_k occurs when no improvement is made for a small enough mesh size,

$$lim_{i\to\infty}||S_i - (S_{i-1} \pm \omega_i e_j)|| = 0, \forall j.$$

Chapter 4

Results and Analysis

4.1 Gradient descent

Figure 4.1 shows the result of running the gradient decent algorithm for a case where we only wish to change the stagger and keeping the span lengths constant is presented.

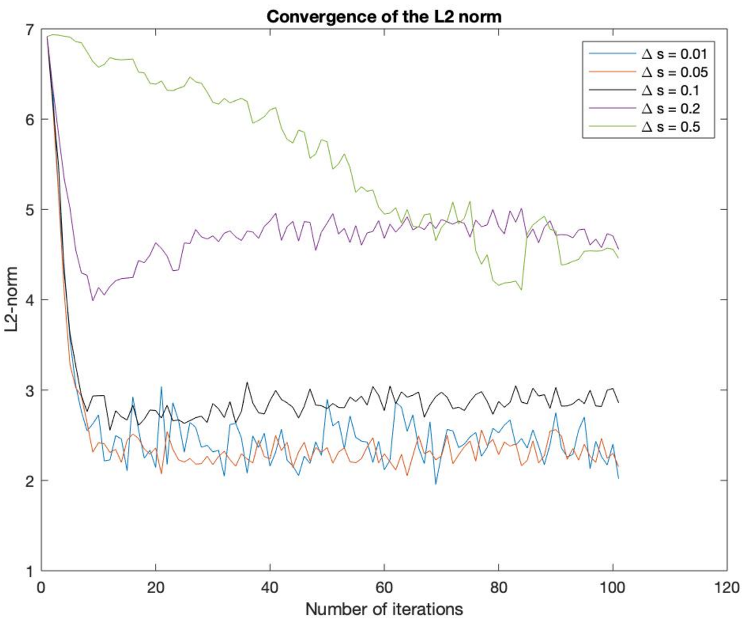

Figure 4.1: Gradient decent convergence for a few different values of Δs and $\gamma = 0.005$

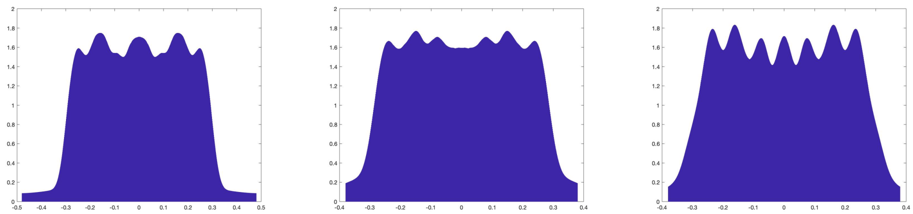

(a) $\Delta s = 0.01$ (b) $\Delta s = 0.05$ (c) $\Delta s = 0.1$

Figure 4.2: Resulting distributions for the three values of Δs that performed the best in Figure 4.1

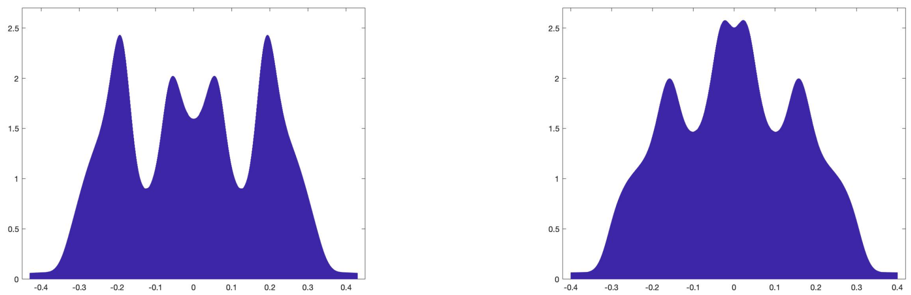

(a) $\Delta s = 0.2$ (b) $\Delta s = 0.5$

Figure 4.3: Resulting distributions for the two values of Δs that performed the worst in Figure 4.1

	Start config.		$\Delta s = 0.01$		$\Delta s = 0.05$		$\Delta s = 0.1$	
Radii	s$_1$	s$_2$	s$_1$	s$_2$	s$_1$	s$_2$	s$_1$	s$_2$
20000	0.300	-0.300	0.301	-0.302	0.280	-0.283	0.257	-0.256
10000	0.300	-0.300	0.299	-0.300	0.282	-0.283	0.290	-0.293
9000	0.300	-0.300	0.297	-0.299	0.286	-0.287	0.313	-0.313
8000	0.300	-0.300	0.299	-0.300	0.280	-0.282	0.290	-0.295
7000	0.300	-0.300	0.298	-0.299	0.279	-0.281	0.291	-0.296
6000	0.300	-0.300	0.297	-0.299	0.274	-0.280	0.253	-0.272
5000	0.200	0.200	0.315	0.315	0.296	0.296	0.334	0.334
4500	0.200	0.200	0.119	0.119	0.220	0.220	0.178	0.178
4000	0.200	0.200	0.311	0.319	0.305	0.305	0.263	0.263
3500	0.200	0.200	0.316	0.481	0.373	0.382	0.375	0.375
3000	0.200	0.200	0.304	0.304	0.314	0.314	0.338	0.325
2500	0.200	0.200	0.295	0.295	0.284	0.284	0.269	0.269
2000	0.300	0.300	0.293	0.293	0.292	0.292	0.321	0.321
1900	0.300	0.300	0.295	0.295	0.275	0.275	0.261	0.261
1800	0.300	0.300	0.294	0.294	0.273	0.273	0.270	0.270
1700	0.300	0.300	0.299	0.299	0.291	0.291	0.298	0.299
1600	0.300	0.300	0.302	0.302	0.288	0.288	0.322	0.322
1500	0.300	0.300	0.307	0.307	0.294	0.294	0.274	0.274
1400	0.300	0.300	0.306	0.306	0.307	0.307	0.298	0.299
1300	0.300	0.300	0.329	0.329	0.299	0.299	0.273	0.274
1200	0.300	0.300	0.247	0.247	0.288	0.288	0.274	0.274

Table 4.1: Updated stagger configurations for the three different good solutions

	$\Delta s = 0.01$		$\Delta s = 0.05$		$\Delta s = 0.1$	
Radii	Wind	Lateral Force(N)	Wind	Lateral Force	Wind	Lateral Force
20000	0.340	(327, -330)	0.330	(309 -211)	0.320	(286, -188)
10000	0.360	(374, -179)	0.350	(358 -163)	0.360	(367, -172)
9000	0.370	(383, -167)	0.360	(373 -156)	0.370	(397, -181)
8000	0.370	(398, -155)	0.360	(381 -138)	0.370	(392, -148)
7000	0.380	(415, -136)	0.370	(398 -119)	0.380	(410, -132)
6000	0.390	(438, -113)	0.380	(418 -94)	0.380	(405, -80)
5000	**0.440**	(195, 195)	**0.420**	(195 195)	**0.460**	(195,195)
4500	0.230	(217, 216)	0.330	(217 217)	0.290	(217, 217)
4000	**0.410**	(247, 247)	0.400	(244 244)	0.360	(244, 244)
3500	**0.500**	(354, 354)	**0.460**	(283 283)	**0.450**	(279, 279)
3000	0.360	(325, 325)	0.370	(325, 325)	0.380	(331, 319)
2500	0.310	(390, 390)	0.300	(390, 390)	0.290	(390, 390)
2000	0.290	(487, 487)	0.290	(487, 487)	0.320	(487, 488)
1900	0.300	(513, 513)	0.280	(513, 513)	0.260	(513, 513)
1800	0.290	(542 541)	0.270	(542, 542)	0.270	(542, 574)
1700	0.300	(573 573)	0.290	(573, 573)	0.300	(573, 574)
1600	0.300	(609, 609)	0.290	(609, 609)	0.310	(609, 609)
1500	0.310	(650, 650)	0.290	(650, 650)	0.330	(650, 650)
1400	0.310	(696, 696)	0.310	(696, 696)	0.310	(696, 696)
1300	0.330	(750, 750)	0.340	(750 ,750)	0.320	(750, 750)
1200	**0.420**	(812, 812)	0.380	(812, 812)	0.400	(812, 813)

Table 4.2: Calculated maximum wind deviation and the lateral force with the values from Table 4.1

In Table 4.2 we see that the 3 different stagger configurations that the Gradient algorithm converged to in Figure 4.1 violate the wind criteria. This means they are not feasible for practical implementation and an improvement is needed.

In Figure 4.4 the L2-convergence for Gradient descent with the modified Algorithm 1 for the wind criteria is presented. In Table 4.3 it is apparent that all Maximum wind deviations stays ≤ 0.4 and the lateral forces for both s_1 and s_2 stays within [70, 900 N]. The resulting distributions for the two values of γ that performed the best are presented in Figure 4.5.

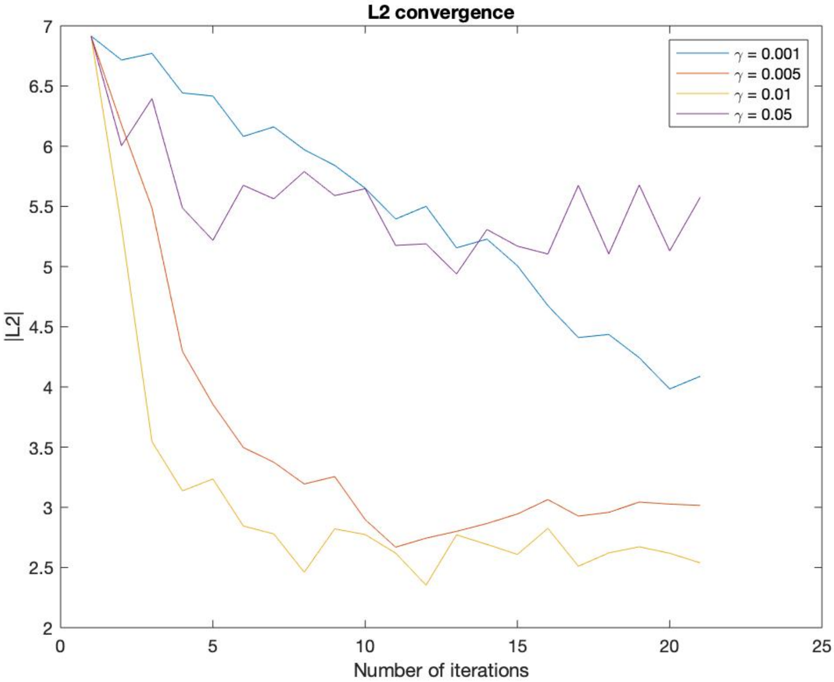

Figure 4.4: L2 convergence for different values of γ and Δ s = 0.1.

$\gamma = 0.01$		$\gamma = 0.005$	
Max Wind	**Lateral force(N)**	**Max Wind**	**Lateral Force(N)**
0.360	(342, -244)	0.360	(342, -245)
0.370	(381, -186)	0.370	(383, -188)
0.370	(387, -170)	0.370	(389, -172)
0.380	(404, -161)	0.380	(406, -162)
0.390	(421, -143)	0.390	(423, -145)
0.400	(448, -123)	0.400	(450, -125)
0.400	(195, 195)	0.400	(195, 195)
0.330	(217, 217)	0.320	(217, 217)
0.390	(244, 244)	0.360	(244, 244)
0.400	(279, 279)	0.400	(279, 279)
0.340	(325, 325)	0.360	(325, 325)
0.250	(390, 390)	0.250	(390, 390)
0.330	(488, 488)	0.330	(488, 488)
0.310	(513, 513)	0.320	(513, 513)
0.320	(542, 542)	0.320	(542, 542)
0.310	(574, 574)	0.310	(574, 574)
0.310	(609, 609)	0.320	(609, 609)
0.330	(650, 650)	0.330	(650, 650)
0.320	(696, 696)	0.310	(696, 696)
0.330	(750, 750)	0.330	(750, 750)
0.350	(813, 813)	0.360	(813, 813)

Table 4.3: Structural limitations for modified gradient descent.

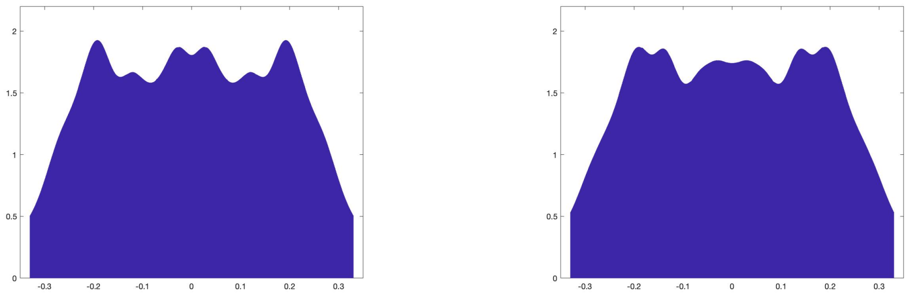

(a) $\gamma = 0.005$ (b) $\gamma = 0.01$

Figure 4.5: Resulting distributions for the two stagger configurations in Table 4.4

	Starting config.		$\gamma = 0.01$		$\gamma = 0.005$	
Radii	s_1	s_2	s_1	s_2	s_1	s_2
20000	0.300	-0.300	0.313	-0.322	0.314	-0.322
10000	0.300	-0.300	0.302	-0.312	0.305	-0.313
9000	0.300	-0.300	0.300	-0.303	0.303	-0.305
8000	0.300	-0.300	0.301	-0.311	0.304	-0.312
7000	0.300	-0.300	0.300	-0.311	0.303	-0.312
6000	0.300	-0.300	0.299	-0.320	0.302	-0.320
5000	0.200	0.200	0.282	0.282	0.282	0.282
4500	0.200	0.200	0.220	0.220	0.213	0.213
4000	0.200	0.200	0.291	0.291	0.260	0.260
3500	0.200	0.200	0.327	0.327	0.327	0.327
3000	0.200	0.200	0.292	0.292	0.310	0.310
2500	0.200	0.200	0.234	0.234	0.230	0.230
2000	0.300	0.300	0.333	0.333	0.329	0.329
1900	0.300	0.300	0.309	0.309	0.315	0.315
1800	0.300	0.300	0.318	0.318	0.325	0.325
1700	0.300	0.300	0.308	0.308	0.312	0.312
1600	0.300	0.300	0.314	0.314	0.320	0.320
1500	0.300	0.300	0.331	0.331	0.335	0.335
1400	0.300	0.300	0.317	0.317	0.314	0.314
1300	0.300	0.300	0.334	0.334	0.328	0.328
1200	0.300	0.300	0.315	0.315	0.307	0.307

Table 4.4: Updated stagger configuration for the distributions shown in Figure 4.5.

4.2 Built in MATLAB Optimizers Results

In this section the function f in Equation (3.4) is optimized using some of Matlabs optimizers suited for Black-Box problems.

All optimizations will be performed on the distribution in Figure 3.8 using real rail network data.

First the GA algorithm was tested for a case where both penalty terms was equal to zero and the search range for the stagger was [-1, 1]. The resulting distribution is shown in Figure 4.6. Note that the algorithm is able to produce a stagger configuration that results in a distribution close to the U(0.3, -0.3) distribution. This tells us that Matlab optimizers are able to perform well. But whats interesting in this section is to find values of the penalty terms that cancels solutions that violate the wind criteria and in addition are able to extend span-lengths. This is the main study in this section.

By increasing the value of K_{wind} to 1000 the GA is able to produce the distribution shown in Figure 4.7 and the updated stagger configuration is presented in Table 4.5. Same goes for the Pattern search algorithm, note how similar the distribution shown in Figure 4.8 is to the one produced by GA.

But looking at Tables 4.5 and 4.7 the stagger configurations vary a lot despite the same starting configurations which are consequently chosen to be the ones used from *SYT-15/15* standard [4]. The starting values for the stagger from Table 2.1, has alternating stagger, (-0.300, 0.300) for radii: 20000, 10000, 9000, 8000, 7000, 6000 m and for all curve radii smaller than this it is unilateral stagger (0.200, 0.200) or (0.300, 0.300). But looking at Tables 4.7 and 4.8 Pattern search additionally optimizes the value of s_2 to negative for the curve radii 5000 and 4500 m, which is positive in *SYT-15/15* standard, implying alternating stagger. The same happens for GA in Table 4.5. Pattern search decreases the first term of equation (3.17) to 2.4, while still preserving a configuration where the deviation with added wind consequently stays within [-0.4, 0.4], mathematically this means that the second and third integrals of equation (3.17) become zero. Ga decreases the same term to 3.3.

Looking at Table 4.5 it is apparent that the GA violates the Lateral force criteria for at least 3 curve radii, this is fixed by increasing the penalty term for the Lateral force K_p to 500. Looking at table 4.6 it is apparent that the penalty term affects the solution.

Comparing tables 4.7 and 4.8 it is apparent that the penalty term K_p has little impact since the Lateral force criteria is already fulfilled with it being set to zero. The conclusion is made that Pattern search is slightly more consistent and robust for this problem.

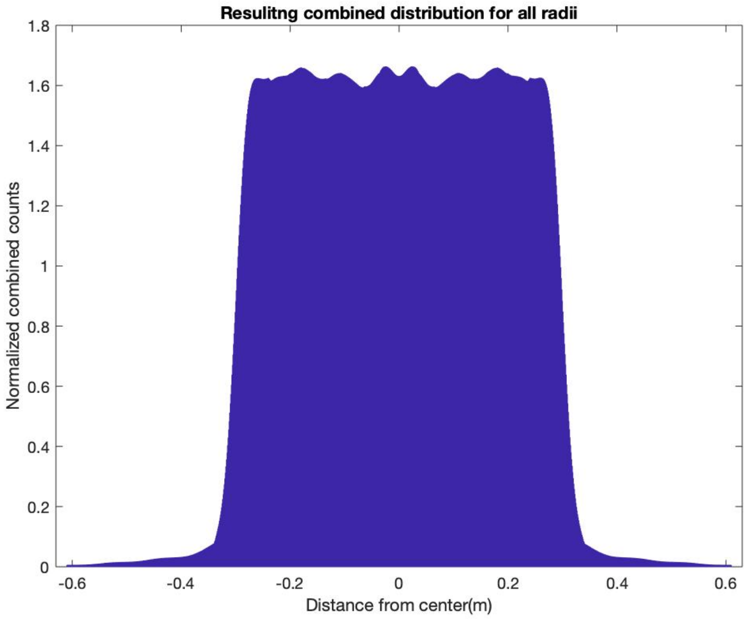

Figure 4.6: Ga $K_{wind} = K_{Sl} = K_p = 0$

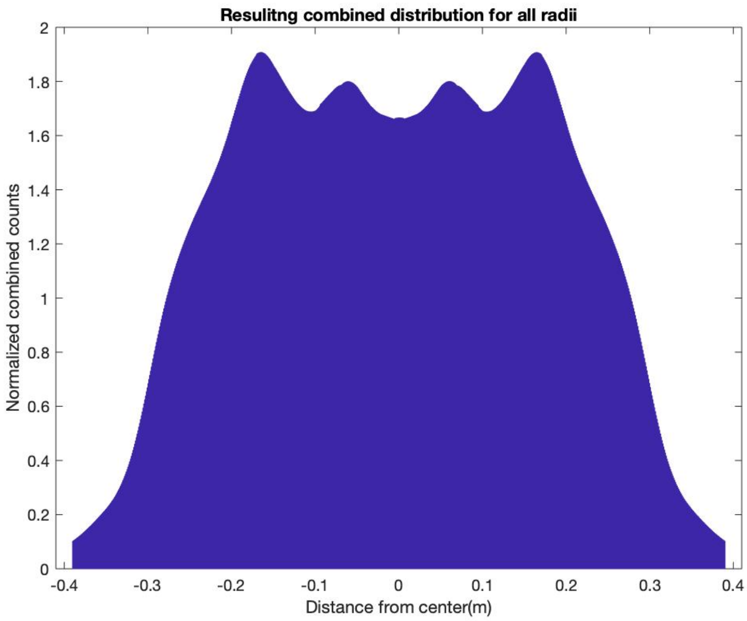

Figure 4.7: Ga $K_{wind} = 1000$, $K_{Sl} = K_p = 0$

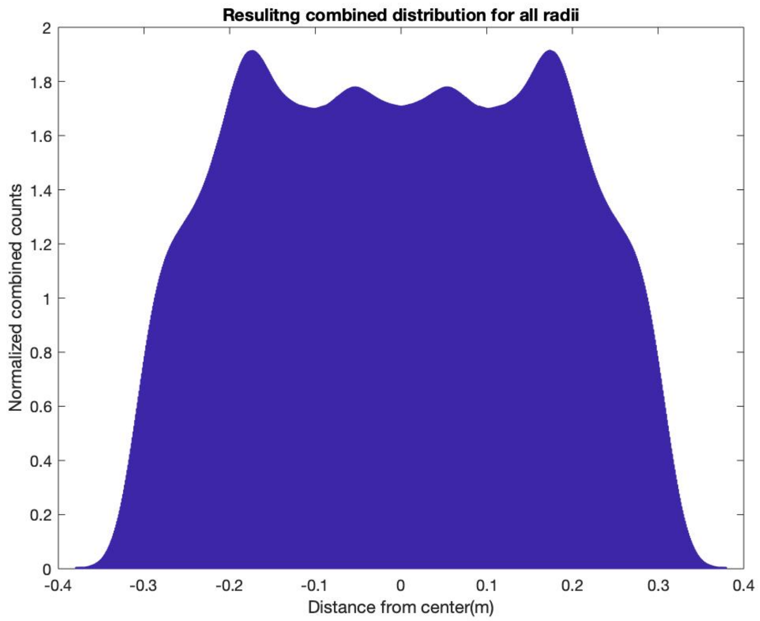

Figure 4.8: Pattern Search $K_{wind} = 1000$, $K_{Sl} = K_p = 0$

		s_1		s_2			
Radii	constant Sl	start	updated	start	updated	**Wind**(m)	Lateral force
20000	65	0.300	0.285	-0.300	0.092	0.40	(138, **-40**)
10000	65	0.300	0.149	-0.300	-0.303	0.40	(306, -111)
9000	65	0.300	0.285	-0.300	0.107	0.38	(190, **26**)
8000	65	0.300	0.156	-0.300	-0.289	0.40	(327, -84)
7000	65	0.300	0.329	-0.300	-0.262	0.34	(412, -133)
6000	65	0.300	0.271	-0.300	0.252	0.40	(171, 154)
5000	65	0.200	0.312	0.200	-0.290	0.39	(473, -83)
4500	65	0.200	0.301	0.200	-0.245	0.37	(469, **-35**)
4000	65	0.200	0.323	0.200	0.257	0.39	(274, 213)
3500	65	0.200	0.295	0.200	0.302	0.38	(275, 282)
3000	65	0.200	0.314	0.200	0.146	0.32	(403, 247)
2500	65	0.200	0.300	0.200	0.365	0.37	(360, 420)
2000	65	0.300	0.177	0.300	0.326	0.33	(419, 556)
1900	65	0.300	0.393	0.300	0.309	0.39	(552, 474)
1800	65	0.300	0.385	0.300	0.319	0.38	(572, 511)
1700	65	0.300	0.294	0.300	0.341	0.34	(552, 595)
1600	65	0.300	0.302	0.300	0.309	0.31	(606, 613)
1500	65	0.300	0.377	0.300	0.361	0.38	(657, 643)
1400	65	0.300	0.331	0.300	0.366	0.37	(680, 713)
1300	65	0.300	0.383	0.300	0.365	0.38	(758, 742)
1200	65	0.300	0.294	0.300	0.387	0.39	(770, 855)

Table 4.5: Optimized Ga, $K_{wind} = 1000, K_{Sl} = K_p = 0$

Radii	Constant Sl	s_1		s_2		Wind	Lateral force (N)
-	-	start	updated	start	updated	-	-
20000	65	0.300	0.306	-0.300	-0.302	0.34	(329, -232)
10000	65	0.300	0.301	-0.300	-0.277	0.34	(364, -169)
9000	65	0.300	0.321	-0.300	-0.292	0.35	(391, -174)
8000	65	0.300	0.296	-0.300	-0.304	0.38	(399, -155)
7000	65	0.300	0.289	-0.300	-0.305	0.38	(413, -135)
6000	65	0.300	0.058	-0.300	-0.115	0.35	(242, 83)
5000	65	0.200	0.185	0.200	0.305	0.31	(140, 250)
4500	65	0.200	0.269	0.200	0.290	0.29	(207, 226)
4000	65	0.200	0.126	0.200	-0.057	0.33	(159, 328)
3500	65	0.200	0.328	0.200	0.267	0.33	(307, 250)
3000	65	0.200	0.378	0.200	0.308	0.38	(357, 293)
2500	65	0.200	0.281	0.200	0.045	0.29	(499, 281)
2000	65	0.300	0.386	0.300	0.380	0.39	(490, 485)
1900	65	0.300	0.371	0.300	0.347	0.37	(524, 502)
1800	65	0.300	0.390	0.300	0.322	0.39	(573, 511)
1700	65	0.300	0.359	0.300	0.398	0.40	(556, 592)
1600	65	0.300	0.302	0.300	0.330	0.33	(597, 622)
1500	65	0.300	0.373	0.300	0.362	0.37	(655, 645)
1400	65	0.300	0.303	0.300	0.295	0.31	(700, 693)
1300	65	0.300	0.307	0.300	0.244	0.36	(779, 721)
1200	65	0.300	0.302	0.300	0.338	0.35	(796, 829)

Table 4.6: Optimized Ga, $K_{wind} = 1000, K_p = 500, K_{Sl} = 0$

		s_1		s_2			
Radii	constant Sl	$start$	$updated$	$start$	$updated$	**Wind**(m)	Lateral force (N)
20000	65	0.300	0.300	-0.300	-0.300	0.34	(326, -228)
10000	65	0.300	0.300	-0.300	-0.300	0.36	(374, -179)
9000	65	0.300	0.300	-0.300	-0.300	0.37	(385, -169)
8000	65	0.300	0.300	-0.300	-0.300	0.37	(399, -155)
7000	65	0.300	0.300	-0.300	-0.300	0.38	(416, -138)
6000	65	0.300	0.300	-0.300	-0.300	0.39	(439, -114)
5000	65	0.200	0.300	0.200	-0.300	0.40	(472, -82)
4500	65	0.200	0.322	0.200	-0.300	0.40	(504, -70)
4000	65	0.200	0.320	0.200	0.231	0.32	(285, 203)
3500	65	0.200	0.307	0.200	0.325	0.32	(270, 287)
3000	65	0.200	0.317	0.200	0.325	0.32	(321, 329)
2500	65	0.200	0.321	0.200	0.200	0.32	(446, 334)
2000	65	0.300	0.050	0.300	0.246	0.35	(397, 578)
1900	65	0.300	0.038	0.300	0.300	0.35	(392, 634)
1800	65	0.300	0.300	0.300	0.300	0.30	(542, 542)
1700	65	0.300	0.301	0.300	0.301	0.30	(574, 574)
1600	65	0.300	0.377	0.300	0.300	0.30	(645, 574)
1500	65	0.300	0.303	0.300	0.300	0.38	(651, 649)
1400	65	0.300	0.299	0.300	0.300	0.33	(696, 697)
1300	65	0.300	0.302	0.300	0.300	0.37	(751, 749)
1200	65	0.300	0.298	0.300	0.300	0.37	(812, 813)

Table 4.7: Optimized Pattern Search, $K_{wind} = 1000, K_p = K_{Sl} = 0$

		s_1		s_2			
Radii	constant Sl	$start$	$updated$	$start$	$updated$	**Wind**(m)	Lateral Force(N)
20000	65	0.300	0.300	-0.300	-0.300	0.34	(326, -228)
10000	65	0.300	0.300	-0.300	-0.300	0.36	(374, -179)
9000	65	0.300	0.300	-0.300	-0.300	0.37	(385, -169)
8000	65	0.300	0.300	-0.300	-0.300	0.37	(399, -155)
7000	65	0.300	0.301	-0.300	-0.300	0.38	(416, -138)
6000	65	0.300	0.300	-0.300	-0.300	0.39	(439, -114)
5000	65	0.200	0.300	0.200	-0.300	0.40	(472, -82)
4500	65	0.200	0.323	0.200	-0.300	0.40	(504, -71)
4000	65	0.200	0.320	0.200	0.231	0.32	(285, 203)
3500	65	0.200	0.307	0.200	0.325	0.32	(270, 287)
3000	65	0.200	0.317	0.200	0.325	0.32	(321, 329)
2500	65	0.200	0.321	0.200	0.200	0.32	(446, 334)
2000	65	0.300	0.050	0.300	0.246	0.35	(397, 578)
1900	65	0.300	0.038	0.300	0.300	0.35	(392, 634)
1800	65	0.300	0.300	0.300	0.300	0.30	(542, 542)
1700	65	0.300	0.301	0.300	0.301	0.30	(574, 573)
1600	65	0.300	0.293	0.300	0.300	0.30	(606, 613)
1500	65	0.300	0.301	0.300	0.301	0.30	(650, 650)
1400	65	0.300	0.377	0.300	0.300	0.38	(732, 661)
1300	65	0.300	0.303	0.300	0.300	0.33	(751, 749)
1200	65	0.300	0.299	0.300	0.300	0.37	(812, 813)

Table 4.8: Pattern Search, $K_p = 500$, $K_{wind} = 1000$, $K_{Sl} = 0$

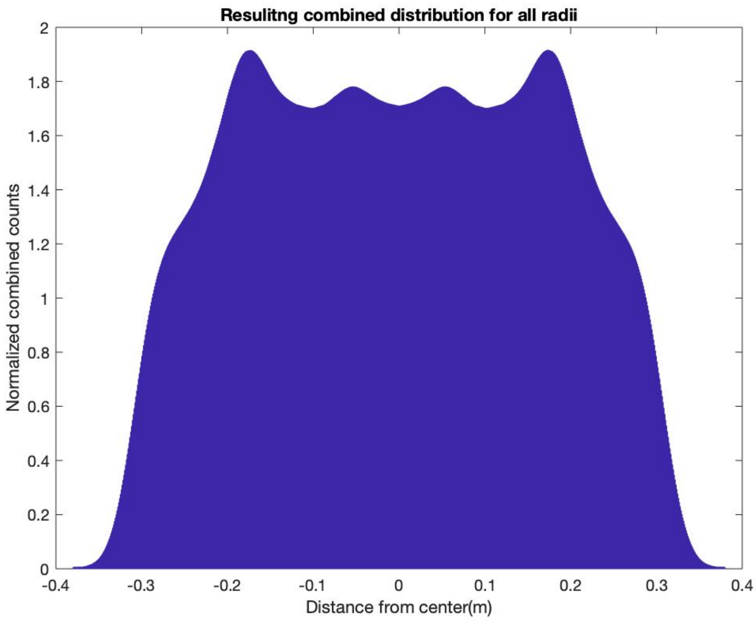

Figure 4.9: Optimized distribution Pattern search, $K_p = 500$, $K_{wind} = 1000$, $K_{Sl} = 0$

Then the value of K_{Sl} was increased to 1000 to favor longer span lengths and the resulting stagger and span lengths are presented in Tables 4.9, 4.11 and their corresponding distributions are presented in Figures 4.11 and 4.10. $'\%'$ refers to the percentage increase of the span lengths. Note that both algorithms are able to find configurations where significant increase in span lengths are apparent without violating the wind- or lateral force 'Drag'-criteria.

	$s_1(m)$		$s_2(m)$		$Sl(m)$				
Curve radii	**start**	**new**	**start**	**new**	**start**	**new**	%	**Wind**	Lateral force
20000	0.300	0.235	-0.300	0.048	65	72	12	0.40	(132, **-24**)
10000	0.300	0.269	-0.300	-0.175	65	71	10	0.33	(294, -81)
9000	0.300	0.170	-0.300	-0.219	65	71	10	0.40	(283, **-46**)
8000	0.300	0.261	-0.300	-0.063	65	83	28	0.40	(273, **39**)
7000	0.300	0.033	-0.300	0.235	65	84	29	0.40	(108, 252)
6000	0.300	0.317	-0.300	-0.031	65	79	23	0.39	(330, **65**)
5000	0.200	0.136	0.200	0.284	65	74	15	0.38	(162, 282)
4500	0.200	0.199	0.200	0.223	65	78	20	0.37	(251, 269)
4000	0.200	0.353	0.200	0.130	65	77	20	0.40	(376, 202)
3500	0.200	0.218	0.200	0.187	65	81	25	0.39	(359, 336)
3000	0.200	0.297	0.200	0.201	65	82	27	0.40	(445, 375)
2500	0.200	0.391	0.200	0.356	65	68	6	0.40	(423, 393)
2000	0.300	0.395	0.300	0.394	65	77	19	0.39	(578, 577)
1900	0.300	0.091	0.300	0.323	65	70	8	0.39	(453, 652)
1800	0.300	0.400	0.300	0.373	65	79	22	0.40	(669, 648)
1700	0.300	0.347	0.300	0.399	65	70	9	0.40	(595, 640)
1600	0.300	0.388	0.300	0.365	65	76	17	0.39	(722, 703)
1500	0.300	0.286	0.300	0.203	65	68	5	0.39	(717, 643)
1400	0.300	0.306	0.300	0.395	65	72	11	0.39	(734, 809)
1300	0.300	0.333	0.300	0.291	63	68	9	0.39	(803, 766)
1200	0.300	0.355	0.300	0.262	62	66	8	0.38	(867, 783)

Table 4.9: Optimized Ga, $K_{wind} = K_{Sl} = 1000$

Lateral force (N)		Wind
s_1	s_2	-
187	-73	0.35
99	128	0.37
-70	302	0.35
210	93	0.37
362	-75	0.31
195	161	0.25
324	156	0.37
403	96	0.37
362	225	0.37
261	400	0.36
250	519	0.38
391	421	0.37
556	478	0.37
667	503	0.40
592	652	0.37
557	714	0.39
651	731	0.40
688	706	0.37
820	824	**0.78**
824	771	0.38
839	884	0.40

Table 4.10: GA Lateral force and wind $K_p = 500$

In table 4.9 it is apparent that the GA violates the Lateral force criteria, setting the penalty term $K_p = 500$ fixes this as seen in table 4.10. But note that for curve radii 1400 the wind deviation is bigger that 0.4m which is not acceptable, even if the penalty term $K_{wind} = 1000$. GA seems to be beaten by the Pattern search algorithm in every aspect.

Comparing tables 4.11 and 4.12 it is clear that the Penalty term K_p have small impact on the Pattern search algorithm. The results between them are almost identical and both are able to ensure both structural limitations (wind and lateral force), while promoting longer Span lengths and ensuring good contact.

	$s_1(m)$		$s_2(m)$		$Sl(m)$				
Curve radii	**start**	**new**	**start**	**new**	**start**	**new**	%	**Wind**	Lateral force
20000	0.300	0.300	-0.300	-0.300	65	74	14	0.40	(299, -188)
10000	0.300	0.300	-0.300	-0.300	65	71	9	0.40	(360, -147)
9000	0.300	0.300	-0.300	-0.300	65	70	8	0.40	(374, -140)
8000	0.300	0.300	-0.300	-0.300	65	69	6	0.40	(390, -131)
7000	0.300	0.300	-0.300	-0.300	65	68	5	0.40	(410, -119)
6000	0.300	0.300	-0.300	0.200	65	67	3	0.30	(212, 123)
5000	0.200	0.200	0.200	0.200	65	83	28	0.35	(249, 249)
4500	0.200	0.216	0.200	0.200	65	86	32	0.40	(292, 281)
4000	0.200	0.278	0.200	0.200	65	84	29	0.36	(343, 287)
3500	0.200	0.341	0.200	0.200	65	82	26	0.34	(403, 300)
3000	0.200	0.309	0.200	0.325	65	79	22	0.32	(389, 401)
2500	0.200	0.372	0.200	0.325	65	85	31	0.40	(527, 493)
2000	0.300	0.378	0.300	0.394	65	82	26	0.40	(609, 621)
1900	0.300	0.394	0.300	0.394	65	81	25	0.39	(639, 639)
1800	0.300	0.347	0.300	0.394	65	79	22	0.40	(640, 676)
1700	0.300	0.300	0.300	0.394	65	74	14	0.40	(615, 691)
1600	0.300	0.394	0.300	0.300	65	76	17	0.39	(750, 675)
1500	0.300	0.300	0.300	0.300	65	71	9	0.39	(710, 710)
1400	0.300	0.300	0.300	0.300	65	70	8	0.40	(750, 750)
1300	0.300	0.300	0.300	0.300	63	68	6	0.40	(785, 785)
1200	0.300	0.300	0.300	0.300	62	66	6	0.39	(825, 825)

Table 4.11: Optimized Pattern Search, $K_{wind} = K_{Sl} = 1000$, $K_p = 0$

	$s_1(m)$		$s_2(m)$		$Sl(m)$				
Curve radii	**start**	**new**	**start**	**new**	**start**	**new**	%	**Wind** (m)	Lateral force
20000	0.300	0.300	-0.300	-0.300	65	74	14	0.40	(299, -188)
10000	0.300	0.300	-0.300	-0.300	65	71	9	0.40	(360, -147)
9000	0.300	0.300	-0.300	-0.300	65	70	8	0.40	(374, -140)
8000	0.300	0.300	-0.300	-0.300	65	69	6	0.40	(390, -131)
7000	0.300	0.300	-0.300	-0.300	65	68	5	0.40	(410, -119)
6000	0.300	0.300	-0.300	0.200	65	67	3	0.30	(212, 123)
5000	0.200	0.200	0.200	0.200	65	83	28	0.35	(249, 249)
4500	0.200	0.216	0.200	0.200	65	86	32	0.40	(292, 281)
4000	0.200	0.278	0.200	0.200	65	84	29	0.36	(343, 287)
3500	0.200	0.341	0.200	0.200	65	82	26	0.34	(403, 300)
3000	0.200	0.309	0.200	0.325	65	79	22	0.32	(389, 401)
2500	0.200	0.372	0.200	0.325	65	85	31	0.40	(527, 493)
2000	0.300	0.378	0.300	0.394	65	82	26	0.40	(609, 621)
1900	0.300	0.394	0.300	0.394	65	81	25	0.39	(639, 639)
1800	0.300	0.347	0.300	0.394	65	79	22	0.40	(641, 676)
1700	0.300	0.300	0.300	0.300	65	74	14	0.40	(653, 653)
1600	0.300	0.394	0.300	0.394	65	76	17	0.39	(713, 713)
1500	0.300	0.300	0.300	0.300	65	71	9	0.39	(710, 710)
1400	0.300	0.300	0.300	0.300	65	70	8	0.40	(750, 750)
1300	0.300	0.300	0.300	0.300	65	68	5	0.40	(785, 785)
1200	0.300	0.300	0.300	0.300	65	66	2	0.39	(825, 825)

Table 4.12: Optimized Pattern Search, $K_{wind} = K_{Sl} = 1000$, $K_p = 500$

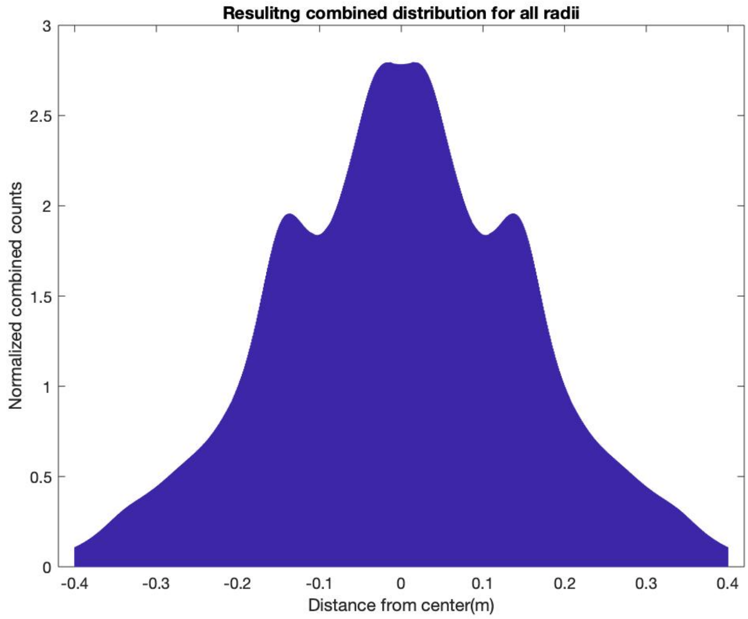

Figure 4.10: Optimized Ga, $K_{wind} = K_{Sl} = 1000$

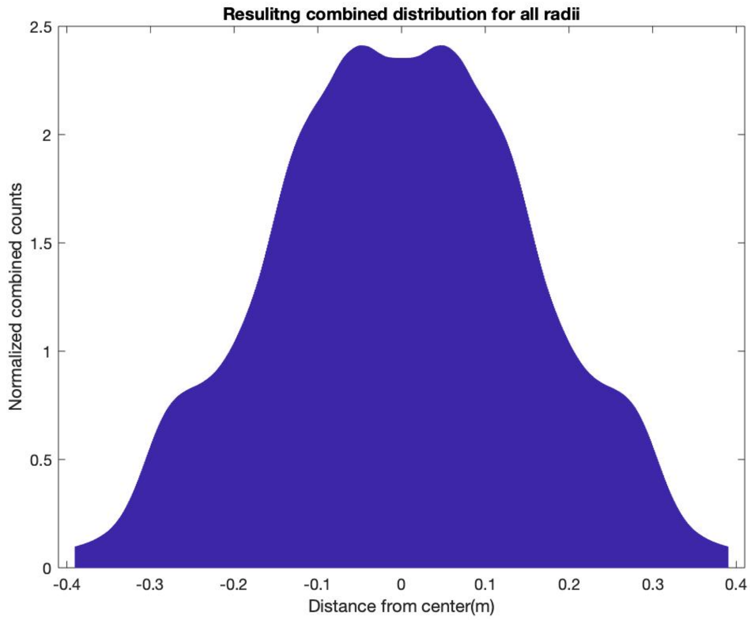

Figure 4.11: Optimized Pattern search, $K_{wind} = K_{Sl} = 1000$

Chapter 5

Discussion

The model for producing the distribution of contact is a versatile ground for understanding and visualizing the complex relationship between the overall wear of the pantograph and the configuration of staggers and span lengths for different curve radii. It is able to take into account all static scenarios such as the impact of wind, different span-lengths, different staggers etc. It gives constructors a visual tool for verifying and understanding the mechanical wear pattern of the pantograph contact strips. The optimization is a tool for distributing the wear more evenly. The gradient descent algorithm presented in chapter 3 and 4 is a powerful tool for distributing the contact points evenly by alternating the stagger configuration, given a constant span length.

The gradient-free optimization that works on equation (3.17) furthermore gives the user the option to alter the span lengths. The penalty constants in equation (3.17) can be chosen in different ways. A value of zero of the penalty constant simply implies that the optimization will only work by alternating the staggers and span lengths to minimize the L2 norm, i.e. making the distribution of contact points uniform or close to that. By increasing K_{Sl} longer span lengths will be favored higher, and by increasing K_{Wind} the chance of obtaining a configuration that may result in a wind parabola of the CW that falls outside of the nominal working zone of the pantograph is reduced. For optimized solutions where the resulting lateral force configurations falls outside of the range [70, 900 N], the penalty term K_p can be increased to punish those 'bad' solutions harder. Note that when using a high value of all penalty terms, K_p, K_{Sl} and K_{wind}, the algorithm's main purpose is to find configurations that enables long span lengths while still ensuring the wind parabola falls within the acceptable range while not abusing the lateral force criteria; hence the algorithm is less prone to find solutions that make the distribution close to uniform, and this is a trade-off you have to make.

The stochastic nature of the Genetic algorithm can affect the convergence rate. Some runs may converge quickly to a high-quality solution, while others might take longer due to exploration of less promising regions. This makes reproducing solutions hard. In contrast, Pattern search is a deterministic algorithm and this makes it easier to reproduce solutions. The modified gradient decent in Algorithm 1 also takes into account a criterion that prohibits stagger configurations that result in lateral forces outside of the domain [70-900 N]. But this was found to be a bit redundant since none of the gradient descent-produced stagger or span length configurations violated this range of accepted values.

It was proven using Patterns search that it is possible to make span lengths longer for some curve radii up to about 30 % which would imply a drastic decrease in production cost and time since it would require fewer posts including their foundations being built.

The overall wear pattern is clearly a complex structure but interestingly using both gradient based and gradient free optimization tools it is possible to find configurations that minimize the wear peaks of the pantograph strip. Furthermore by altering stagger configurations it is possible to build longer span lengths that still ensure a good lateral point of contact. Overall Gradient decent did not alter the stagger configurations as drastically as the two gradient-free optimization techniques, partly due to the fact that it was limited to altering stagger only whilst the other two could alter the span lengths. But, it may be an indication that gradient-free techniques are preferable for this problem. According to [5], span lengths are usually prominently limited by: wind loads, curves and short pantograph strips. Since all of these are included in the static evaluations in this paper, that is a solid ground for further dynamic investigation.

Chapter 6

Conclusions and Future work

6.1 Conclusions

Using both gradient-based and gradient-free optimizing algorithms it is possible to spread the point of contact distribution, measured in contact per time, between the CW and the pantograph contact strip for electric rail vehicles. It is possible to alter span lengths and staggers in order to make the contact distribution closer to uniform and it is also possible to increase the span lengths while still preserving a good lateral contact distribution. These configurations need to be validated dynamically with regards to the elasticity and contact force they imply, in order to be practically eligible. Both the Gradient decent method and the gradient-free techniques were able to produce solutions that converged to at least local optima, since the exact nature of the objective function is unknown we cannot say that they in fact are global optima.

6.2 Limitations

The wear pattern of a pantograph will be strongly dependent on the contact force between the contact strip and the CW. Usually the force is bigger at the supports which corresponds to specific lateral positions, therefore the wear pattern might look different than the lateral contact pattern in this paper. The wear of the pantograph is a mixture between mechanical adhesive wear due to friction and wear due to electrical current flow between the pantograph and the catenary wire, such as burning arc and thermal wear from the heat generated by the current. All of these are certainly strongly dependent on the actual point of contact onto the contact strip, but the adhesive wear will be more prominent at points where the contact force is bigger [9].

The Genetic algorithm is a stochastic iterative algorithm which means that results might vary from time to time. Also, the algorithm is rather slow, faster Black-Box algorithms might exist.

The angle of the SE will affect the working zone of the contact strip according to Figure 6.1. The highest superelevation used in Sweden is approximately 160 mm, and for the track gauge of 1435 mm this means $\alpha = arcsin(\frac{160}{1435})$. With working zone = absolute width $\cdot cos(\alpha)$ and assuming absolute working zone width of the contact strip being [-0.4, 0.4] as in this report the working width needs to be reduced to [-0.3975, 0.3975] in order to take into account that extreme case. Furthermore, with SE apparent the center of the pantograph will not align with the center of the track gauge, which is assumed in this work. Assuming a height of 5.5 m from the track to the CW, which is a common value of the height of the CW, the center point of the Pantograph collector-strip would be decreased by

$$\Delta R = 5.5 \cdot tan(\alpha) \approx 0.62m.$$

Hence, the the radii would need to be decreased to $R - \Delta R$ in those sections and the stagger values would need to be shifted inward accordingly.

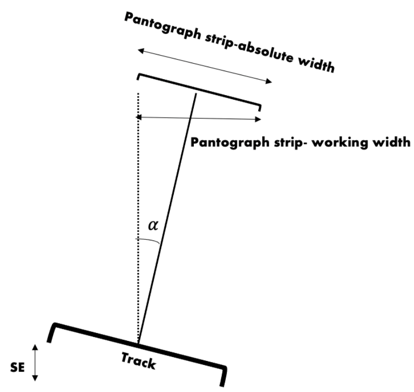

Figure 6.1: Superelevation

Furthermore the bin representation used to produce the distributions might have an offset of about 0.005 m since the bin width used to produce the distributions in the optimization are fixed to 0.01 m, same as the diameter of the CW. This limitation also applies to the wind evaluation. Wind deviations that exceed the limit 0.4 m with less than 0.005 m (half the bin width) might be accepted meaning that some of the optimized stagger and span length configurations might result in wind deviations in the range [0.40 0.405 m] that are evaluated as equal to 0.4 m.

6.3 Future work

Possible future work could include:

- -Dynamically validating the stagger and span-length configurations using FEM-based programs.

- -Validating the stagger and span length configuration with regards to the lateral speed they imply [9].

- - Take into account the inclination angle, SE, used in curved train sections, since this might affect both the point of contact and the working width of the tilted pantograph. [5]

- -Trying different gradient-free optimization techniques.

References

[1] P. Antunes, J. Ambrósio, J. Pombo, and A. Facchinetti, "A new methodology to study the pantograph–catenary dynamics in curved railway tracks," *Vehicle System Dynamics*, 2020. [Pages ix and 2.]

[2] C. EU, "Technical specifications for interoperability relating to the energy subsystem of the rail system in the union," *Official Journal of the European Union*, vol. 1301, 2014. [Pages 4 and 11.]

[3] Reijm, *Lärobok Kontaktledning*. Banverket, 2006. [Pages ix, 4, 9, 10, and 14.]

[4] *RÅD till KRAV TRVINFRA-00144*. [Pages xi, 7, and 40.]

[5] F. Kiessling, R. Puschmann, A. Schmieder, and E. Schneider, *Contact lines for electric railways: planning, design, implementation, maintenance*. John Wiley & Sons, 2018. [Pages 9, 54, and 57.]

[6] S. Ruder, "An overview of gradient descent optimization algorithms," *arXiv preprint arXiv:1609.04747*, 2016. [Page 26.]

[7] A. Lambora, K. Gupta, and K. Chopra, "Genetic algorithm-a literature review," in *2019 international conference on machine learning, big data, cloud and parallel computing (COMITCon)*. IEEE, 2019, pp. 380–384. [Page 29.]

[8] V. Torczon, "On the convergence of pattern search algorithms," *SIAM Journal on optimization*, vol. 7, no. 1, pp. 1–25, 1997. [Page 30.]

[9] S. Derosa, P. Nåvik, A. Collina, G. Bucca, and A. Rønnquist, "Contact point lateral speed effects on contact strip wear in pantograph–catenary interaction for railway operations under 15 kv 16.67 hz ac systems," *Wear*, vol. 486, p. 204103, 2021. [Pages 55 and 57.]

[10] R. H. Byrd, J. C. Gilbert, and J. Nocedal, “A trust region method based on interior point techniques for nonlinear programming,” *Mathematical programming*, vol. 89, pp. 149–185, 2000.

[11] N. Zhou, Y. Cheng, X. Zhang, X. Zhi, and W. Zhang, “Wear rate and profile prediction of cu-impregnated carbon strip for high-speed pantograph,” *Wear*, vol. 530, p. 205056, 2023.

[12] K. Terayama, M. Sumita, R. Tamura, and K. Tsuda, “Black-box optimization for automated discovery,” *Accounts of Chemical Research*, vol. 54, no. 6, pp. 1334–1346, 2021.

[13] M. Reijm, *Systembeskrivning Hängverksberäkningar*. Banverket, 2002.

[14] E. D. Dolan, R. M. Lewis, and V. Torczon, “On the local convergence of pattern search,” *SIAM Journal on Optimization*, vol. 14, no. 2, pp. 567–583, 2003.

[15] B. Schick, W. Liu, and S. Stichel, “Convergence study for the simulation of stitched railway catenary dynamics and design verification of a high-speed system for sweden,” 2024.

[16] P. Nåvik, A. Rønnquist, and S. Stichel, “Variation in predicting pantograph–catenary interaction contact forces, numerical simulations and field measurements,” *Vehicle System Dynamics*, vol. 55, no. 9, pp. 1265–1282, 2017.

TRITA – SCI-GRU 2025:353
Stockholm, Sweden 2025

www.kth.se